ELSEVIER

Quaternary Science Reviews 27 (2008) 602–620

QSR

A tephra chronostratigraphic framework for the Frontier Mountain blue-ice field (northern Victoria Land, Antarctica)

Pietro Curzio[a], Luigi Folco[a,*], Marinella Ada Laurenzi[b], Marcello Mellini[c], Antonio Zeoli[a]

[a]*Museo Nazionale dell'Antartide, Università di Siena, Via Laterina 8, 53100 Siena, Italy*
[b]*Istituto di Geoscienze e Georisorse, CNR - Area della Ricerca di Pisa, Via G. Moruzzi 1, 56124 Pisa, Italy*
[c]*Dipartimento di Scienze della Terra, Università di Siena, Via Laterina 8, 53100 Siena, Italy*

Received 4 May 2007; received in revised form 20 November 2007; accepted 23 November 2007

Abstract

Englacial tephra provide chronostratigraphic markers in the Antarctic ice sheets. Structural, mineralogical, geochemical and geochronological data on selected samples allowed the reconstruction of a chronostratigraphic framework for the Frontier Mountain blue-ice field—an important meteorite trap on the southeastern flank of Talos Dome in northern Victoria Land. The stratigraphic thickness of the blue-ice succession is ~1150 m. The ^{40}Ar–^{39}Ar age of one layer close to the stratigraphic bottom of the ice succession is 100 ± 5 ka and constrains the maximum age of the bulk of Frontier Mountain blue ice. The 49 ± 11 ka age of a second layer at a depth of ~950 m in the stratigraphic succession indicates that >90% of the ice is younger than this value. These ages agree well with the terrestrial ages of meteorites found on the blue ice (up to 140 ± 30 ka), suggesting a mechanism of exhumation of meteorites by ablation after englacial transport. Particle size (up to several tens of microns) and the alkaline compositional character of 22 layers allow correlation with source volcanoes within the Cenozoic magmatism associated with the West Antarctic Rift System. The proximal Mount Melbourne, Mount Rittman and The Pleiades (within a radius of ~250 km) are the best candidate source volcanoes. The reconstructed chronostratigraphic framework thus lays the foundations for a detailed investigation of ~100 ka of explosive volcanism in northern Victoria Land. Furthermore, in light of the ongoing ice core drilling project at Talos Dome, the Frontier Mountain ice succession may become important for establishing regional correlations, for sampling and dating key tephra layers, and for selecting ice successions for high-resolution studies of past atmospheric chemistry and fallout.
© 2007 Elsevier Ltd. All rights reserved.

1. Introduction

Blue-ice fields are peculiar features of the Antarctic ice sheets that extend for tens to thousands of km^2, accounting for 1% of the surface of the Antarctic continent (Bintanja, 1999). Blue-ice fields often form close to bedrock obstacles to ice flow (mountains, nunataks, shallow bedrock rises). They are characterized by a negative surface mass-balance due to high ablation rates which induces exhumation of deep ice. Blue-ice fields are of great interest to the scientific community for their extraordinary meteorite concentrations (e.g., Cassidy et al., 1992; Harvey, 2003); they are also of potential interest because they represent natural "windows" into the relatively old ice of the Antarctic ice sheets, thus providing easy access to paleoenvironmental records which are complementary to those from ice cores (Bintanja, 1999). Reconstructing the chronostratigraphy of ice in blue-ice fields is a prerequisite for their use as archives of past atmospheric chemistry and fallout.

Tephra layers occur embedded in the Antarctic ice sheets. They are commonly found in ice cores, including the Byrd (which hosts more than 2000 tephra; Gow and Williamson, 1971; Kyle et al., 1981; Palais, 1985; Palais et al., 1988; Hammer et al., 1997), Dome Fuji (Fujii et al., 1999), Dronning Maud Land (Higashi and Fujii, 1994), Vostok (Kyle et al., 1982, 1984; Palais et al., 1989; Basile, 1997; Basile et al., 2001), Dome C (Kyle et al., 1981; Narcisi et al., 2005), Law Dome (Kurbatov et al., 2003), Talos Dome (Narcisi et al., 2001), Taylor and Siple Dome (Dunbar et al., 2003) ice cores. Tephra layers have been documented in the Skelton Nevè and Kempe Glacier

*Corresponding author. Tel.: +390 577 233 892; fax: +390 577 233 890.
E-mail address: folco@unisi.it (L. Folco).

0277-3791/$ - see front matter © 2007 Elsevier Ltd. All rights reserved.
doi:10.1016/j.quascirev.2007.11.017

(Keys et al., 1977), Yamato Mountains (Katsushima et al., 1984; Nishio et al., 1985; Koeberl, 1990), Lewis Cliff (Koeberl, 1988; Koeberl et al., 1988) and Allan Hills (Marvin, 1986; Dunbar et al., 1995; Harvey et al., 1998), Frontier Mountain and Lichen Hills (Perchiazzi et al., 1999), and Mount Moulton (Wilch et al., 1999) ice fields. Tephra layers are isochronous planes of the Antarctic ice sheets which correlate across wide distances (Smellie, 1999), possibly up to hundreds of kilometers, or more. As such, they have long been regarded as potential chronostratigraphic markers of the Antarctic ice sheets (Dunbar et al., 1995; Smellie, 1999; Wilch et al., 1999; Narcisi et al., 2006), possibly enabling reconstruction of ice successions up to a regional scale and providing independent age constraints for glaciological modeling of core timescales.

We present a structural, morphometrical, geochemical and ^{40}Ar–^{39}Ar geochronological study of selected tephra layers from the Frontier Mountain blue-ice field—a well-known meteorite trap in northern Victoria Land (Delisle et al., 1989; Folco et al., 2002). Tephra layers were mapped and sampled during the 1995, 1997, 1999 and 2001 Antarctic Campaigns of the Italian *Programma Nazionale delle Ricerche in Antartide* (PNRA). This work defines the overall structure of the ice body in the area, providing a stratigraphic framework of the ice and a maximum age for the reconstructed ice succession. Implications for regional-scale stratigraphic correlations and meteorite trapping mechanism are also discussed.

2. Glaciological outline

Many glaciological data collected for the study of the meteorite concentration mechanism are available for the Frontier Mountain blue-ice field (Folco et al., 2002). Frontier Mountain (~72°59′S, 160°20′E) is a nunatak within the Transantarctic Mountains, located at the edge of the polar plateau (Outback Nunataks region) in the inland catchment of the upper Rennick Glacier (Fig. 1). It is a 9 km long and 2804 m high, NW–SW trending ridge built up by granitoids, pegmatites and aplites of the Granite Harbor intrusive complex (Gunn and Warren, 1962), which rises for ~600 m above the ~2200 m regional ice level. On its regional northeastward path from the Polar Plateau towards the outlet Rennick Glacier, ice flows past both ends of Frontier Mountain at velocities in excess of 1 m yr^{-1}. Downstream of Frontier Mountain, turbulent south-southwesterly katabatic winds form a ~40 km^2

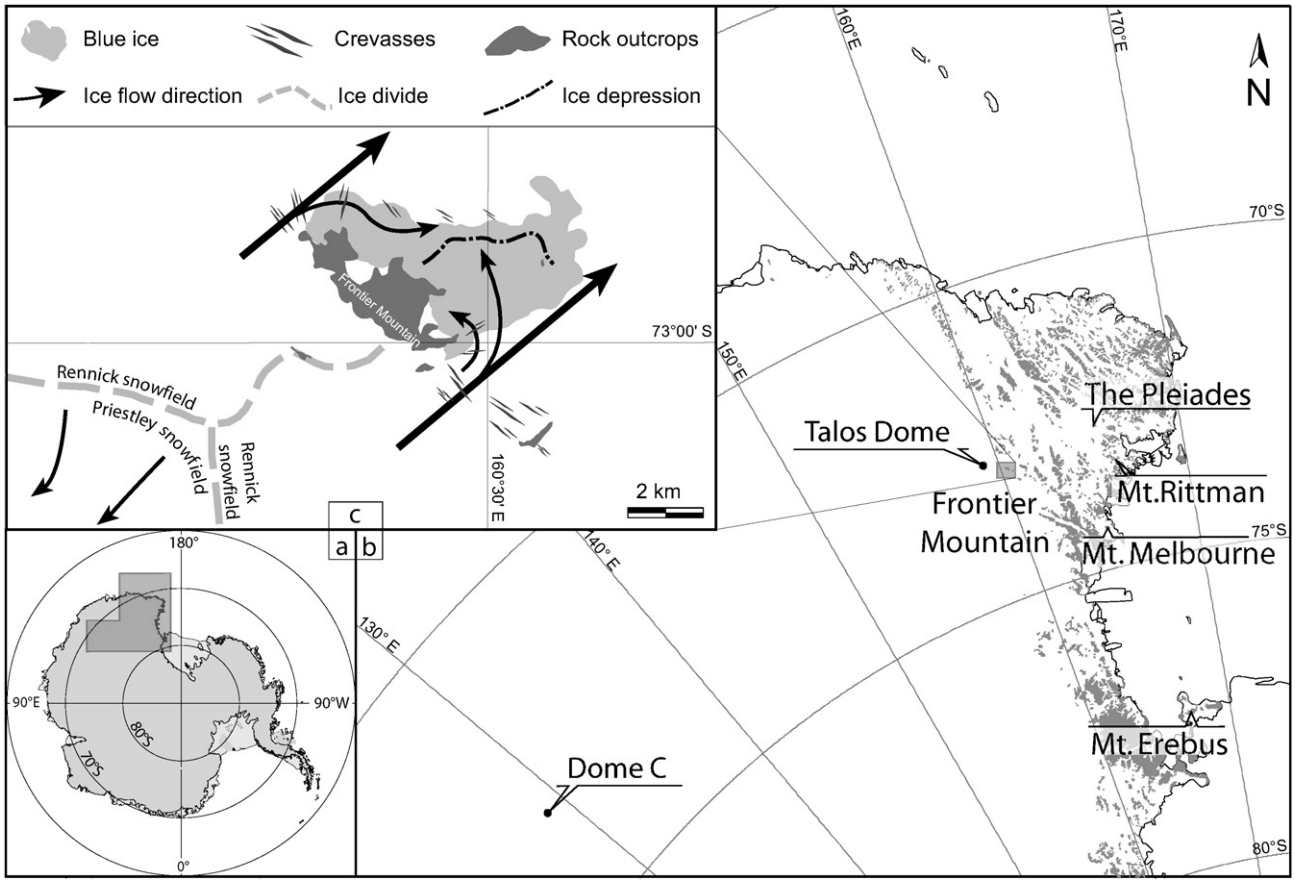

Fig. 1. (a) Sketch map of Antarctica showing the location of the study area. (b) Location map of the Frontier Mountain blue-ice field relative to Dome Concordia (Dome C), Talos Dome, and the McMurdo Volcanic Group emission centers (i.e., The Pleiades, Mt. Melbourne, Mt. Rittman and Mt. Erebus) discussed in this article. (c) Sketch map of the ice flow in the Frontier Mountain area.

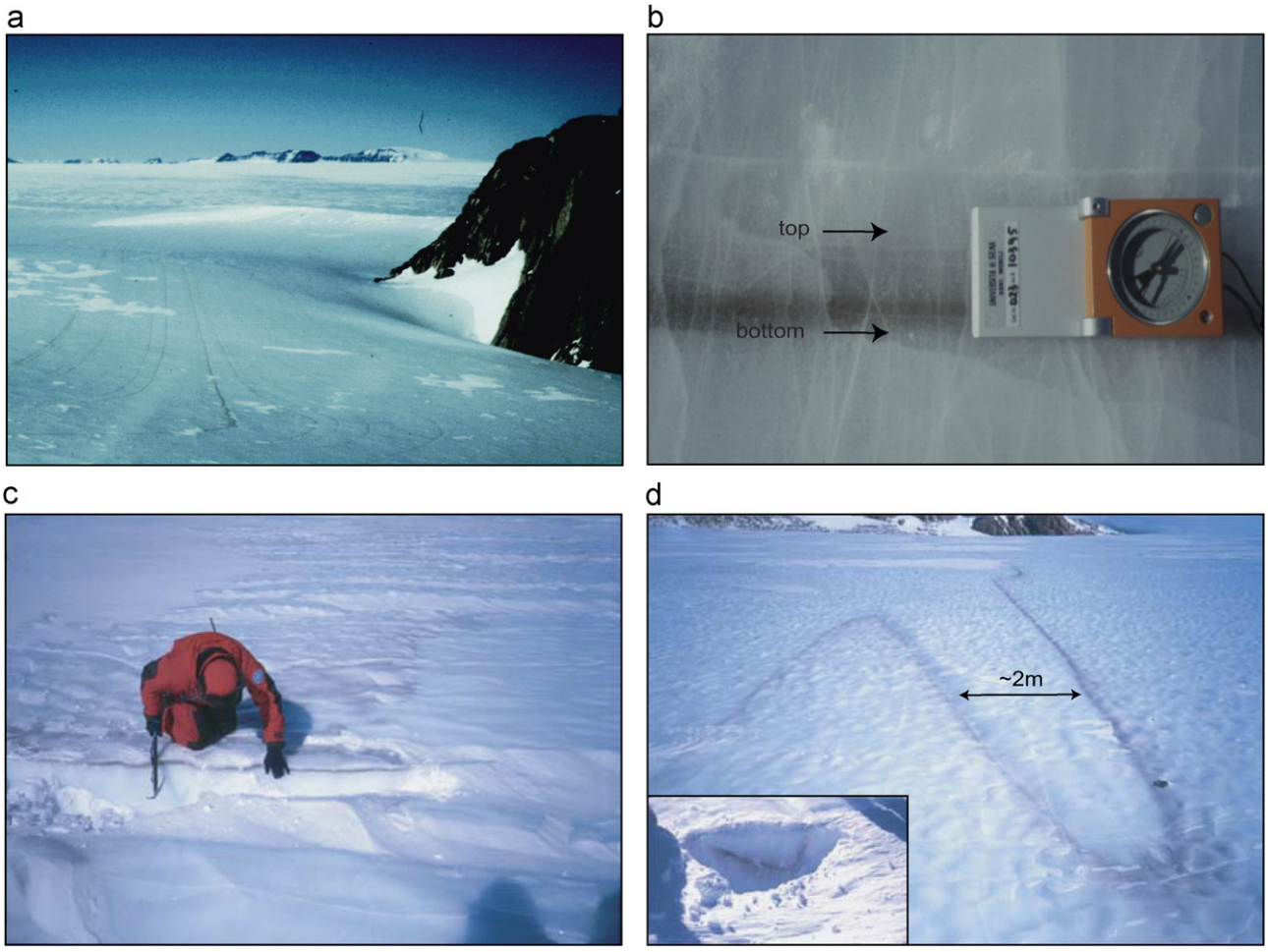

Fig. 2. Tephra layers as they appear at the ice surface: (a) helicopter view of the ZA series cropping out on the northern slope; (b) strike measurement on an almost vertical tephra layer; (c) horizontal layer sampled in a small crevasse; and (d) folded layer as seen on the blue-ice surface and in section (see trench in the inset).

blue-ice area which undergoes relatively high ablation (avg. $6.5 \pm 2\,\mathrm{cm\,yr^{-1}}$). The ice removed by ablation is replenished by ice from the Polar Plateau which flows around both ends of the mountain. The two ice flows meet along a shallow (less than a few tens of meters below the average altitude of the blue-ice field of ~2070 m), east–west trending, curvilinear ice depression. As such, the overall topography of the blue-ice field can be described as a shallow, east–west trending ice valley whose flanks are the fronts of the southern and northern ice flows. The ice depression runs over a shallow (~100–200 m below ice surface) sub-ice bedrock crest. Horizontal velocities of the ice decrease to $<10\,\mathrm{cm\,yr^{-1}}$ on approaching the submerged obstacle, giving rise to a meteorite stranding surface. An ice divide located 15–20 km due west of Frontier Mountain on the southeastern flank of Talos Dome (72°47′14″S, 159°04′2″E; 2318 m WGS84 elevation; ~60 km due northwest of Frontier Mountain; Frezzotti et al., 2004) limits the drainage area of the Frontier Mountain ice field.

Several tens of englacial tephra layers are exposed in the blue-ice field, at the fronts of both the northern and southern ice flows. They crop out as cm-thick, dark, dusty bands which mark the surface of the ice field for up to several kilometers, highlighting the ice stratigraphy and deformation of the ice flows (Fig. 2).

3. Materials and methods

3.1. Mapping and sampling

In order to obtain the overall structural and stratigraphic information on the two ice flows supplying the Frontier Mountain ice field, major tephra layers were mapped on both the northern and southern flanks of the valley (Fig. 3), refining the sketch-map of Perchiazzi et al. (1999).

The geometry of the tephra layers at the blue-ice surface was determined through continuous GPS positioning of their outcrops and measurements of their strike and dip at selected sites. In absence of snow cover, it was possible to continuously track many tephra layers for kilometers. Altitude was determined by GPS receivers and barometric altimeters. During data acquisition, positions and altitudes were repeatedly checked with reference to the geodetic

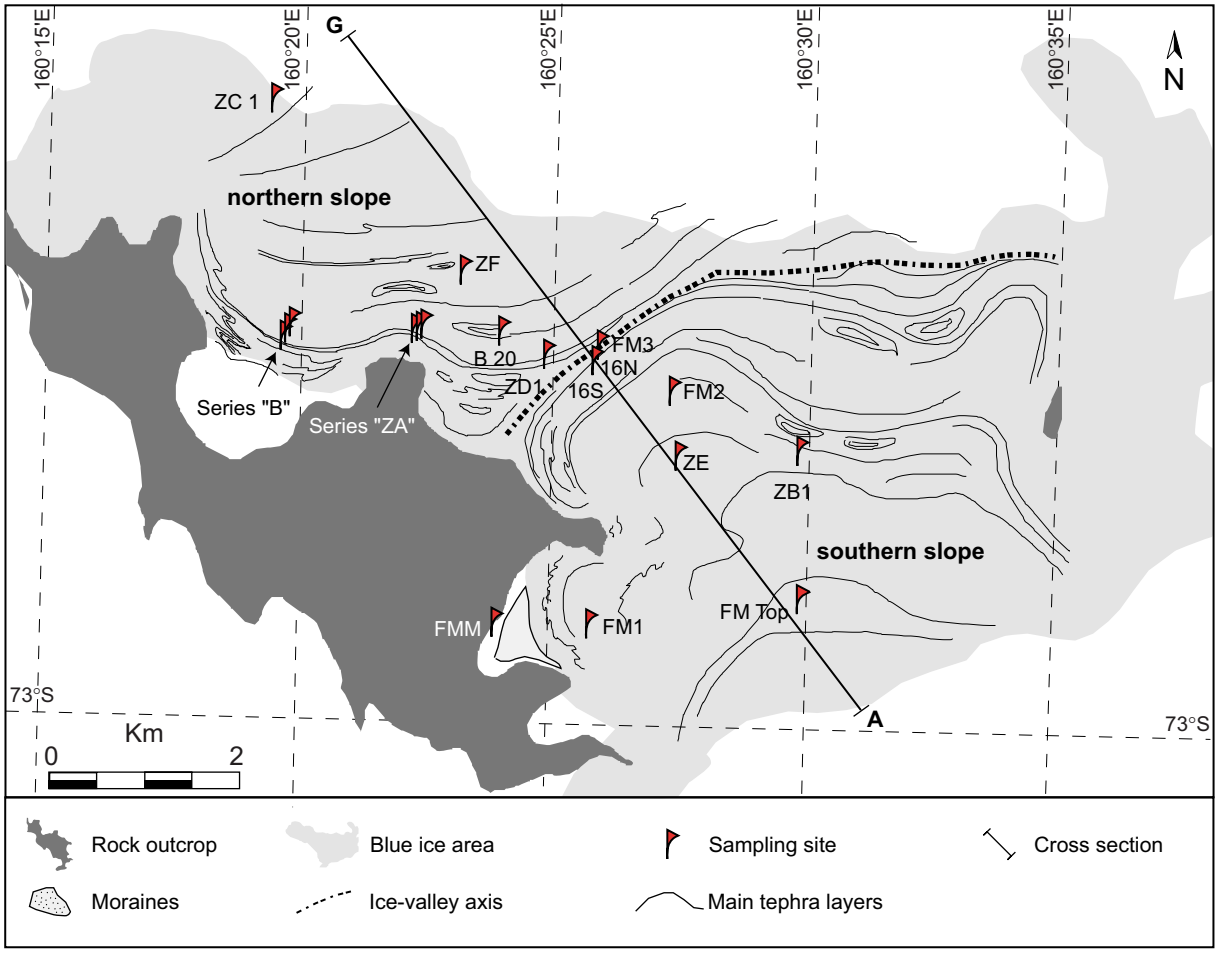

Fig. 3. Map of the Frontier Mountain blue-ice field, with sample locations, major tephra layer contours and indication of the sampling sites. Tephra layer ZD1 is the base (oldest) and ZC1 the top (youngest) of the northern slope sequence; FM3 is the base (oldest) and FM Top the top of the southern slope sequence.

strain-net network installed at the Frontier Mountain blue-ice field (Folco et al., 2002).

All field data were merged and integrated with remote sensing data. Although tephra layers are too small to be detected in Landsat satellite images, the banding of the ice visible in false-color composite reflects the ice stratigraphy. Such information thus provided further insight into the internal structure of the Frontier Mountain blue ice.

Twenty-two of the largest and best exposed tephra layers were sampled from the northern and southern slopes of the ice valley, by collecting 2–20 kg of tephra-bearing ice per layer using a chain-saw or ice-hammer (Fig. 3 and Table 1). On the northern slope, we sampled layers from the northern margin of the blue-ice field (samples ZC1 and ZC1bis) and towards the valley bottom (ZF, B20, and ZD1). Samples were also collected from two series of closely spaced layers (ZA and ZB series) at the foot of the mountain. The ZA3 layer was tracked for some kilometers and sampled a second time close to the ice depression (sample name: ZD1) to check the homogeneity of mineralogical, geochemical and morphometrical features. On the southern slope, tephra layers were sampled from the southern margin of the blue-ice field (FMTop) towards the valley bottom (ZB1, ZE, FM2, 16S, 16N, and FM3). Two more layers were sampled close to the foot of the mountain: one from the ice approaching the Meteorite Valley (FM1) and the other one from the ice at the core of the Meteorite Valley (FMM).

3.2. Laboratory analyses

Tephra separated from melted ice samples by vacuum-filtering through 2 μm mesh filters were dried in an oven for 24 h at 60 °C. The recovered mass for each tephra layers was of the order of 1–10 g. The amount of ash deposited in the unit surface calculated for the thickest layer was 80 g m^{-2}.

For each tephra, a 1 g aliquot was used to produce glass beads for the determination of the bulk chemical composition by X-ray fluorescence (XRF). Smaller aliquots were embedded in epoxy, sectioned and polished for morphometric and mineralogical characterization of the constituent particles, under a PHILIPS XL30 scanning electron microscope equipped with an energy-dispersive

Table 1
Field data for the tephra layers in the Frontier Mountain blue-ice field

Sample	Sampling year	Latitude S	Longitude E	Elevation WGS84 (m)	Dip and dip angle
Northern slope					
ZC1	1999	72°56′21″	160°19′12″	2114	315 (5°)
ZC1bis	2001	72°56′32″	160°17′27″	2154	300 (5°)
ZF	2001	72°57′29″	160°23′06″	2068	280 (30°)
B20	1997	72°57′47″	160°23′59″	2070	240 (35°)
B19	1997	72°57′47″	160°20′07″	2070	240 (35°)
B17	1997	72°57′48″	160°20′06″	2070	240 (35°)
B16	1997	72°57′48″	160°20′03″	2070	240 (35°)
B1	1997	72°57′50″	160°19′56″	2070	240 (35°)
ZA1	1999	72°57′48″	160°22′05″	2065	285 (75°)
ZA2	1999	72°57′48″	160°20′06″	2065	285 (75°)
ZA3	1999	72°57′48″	160°20′07″	2065	285 (75°)
ZA4	1999	72°57′48″	160°20′08″	2065	285 (75°)
ZA8	1999	72°57′48″	160°20′10″	2064	285 (75°)
ZA9	1999	72°57′48″	160°20′11″	2064	285 (75°)
ZA21	1999	72°57′49″	160°22′16″	2063	285 (75°)
ZD1	1999	72°57′55″	160°25′04″	2065	305 (55°)
Southern slope					
FMTop	1999	72°59′19″	160°29′43″	2114	170 (10°)
ZB1	1999	72°58′29″	160°29′50″	2093	170 (10°)
ZE	2001	72°58′24″	160°27′29″	2080	130 (15°)
FM1	1995	72°59′31″	160°25′46″	2093	105 (85°)
FM2	1995	72°58′09″	160°27′17″	2073	110 (30°)
16S	2001	72°57′56″	160°26′01″	2060	130 (70°)
16N	2001	72°57′56″	160°26′01″	2060	130 (70°)
FMM	2001	72°59′39″	160°23′47″	2020	[a]
FM3	1995	72°57′55″	160°26′06″	2059	135 (80°)

Layers from the northern and the southern slopes are ordered from proximal (oldest—base of the section) to distal (youngest—top of the section) with respect to ice valley axis.
[a]Extremely folded layer.

spectrometer (SEM–EDS). Morphometrical parameters were quantitatively analyzed on digitized backscattered electron images, using the "Image Pro Plus" software. Owing to its ubiquitous presence, glass was chosen as a key petrographic feature for the characterization of tephra layers; its major element composition was determined with a JEOL JXA 8600 electron microprobe at the CNR Istituto di Geoscienze e Georisorse in Florence. Running conditions were 15 kV accelerating voltage, 10 nA beam current. Counting time was 10 s for Na and K, and 15 s for the other analyzed elements. A 5–15 μm-diameter defocused beam was employed according to grain size to reduce migration of volatile elements. The Bence and Albee (1968) method was employed for data correction. Synthetic, mineral and glass standards were used for instrumental calibration. The concentrations of 26 trace elements in the glass shards of four tephra layers (FM2, FM3, B19 and B20) were determined by laser ablation–inductively coupled plasma–mass spectrometry (LA–ICP–MS) at the CNR Istituto di Geoscienze e Georisorse in Pavia. The adopted instrument couples a Nd:YAG laser operating at 266 nm with a quadrupole ICP–MS (Drc-e, Perkin-Elmer). Analyses were carried out with a spot 20–50 μm in diameter and NIST SRM 610 and ^{29}Si as external standards. ^{40}Ar–^{39}Ar analyses of seven samples from the northern and southern ice flows (ZC1bis, ZE, B20, ZD1, FM3, 16S, FMTop) were performed at the CNR Istituto di Geoscienze e Georisorse in Pisa. Geochronological data were obtained through the total fusion and step-heating experiments of aliquots of glass and feldspars (typically, alkali feldspars and plagioclase) separates. The analytical procedure, experimental data and interpretations are detailed in the Supplementary Material.

4. Results

4.1. Field description

Tephra appear as dark layers, up to ~2 cm thick, composed of dark particles dispersed within the ice (Fig. 2). Individual layers may consist of several parallel, thin laminae (Fig. 2b). The color of the stratigraphic bottom contrasts sharply with that of the surrounding ice, whereas the top often appears shaded, gradating into the colorless ice. The color of layers ranges from pale-brown to black, depending mainly on the concentration of volcanic ash particles. The spacing of successive tephra layers on the blue-ice surface ranges from decimeters to hundreds of meters. Successions of closely spaced tephra layers are common; for instance, the ZA-series consists of

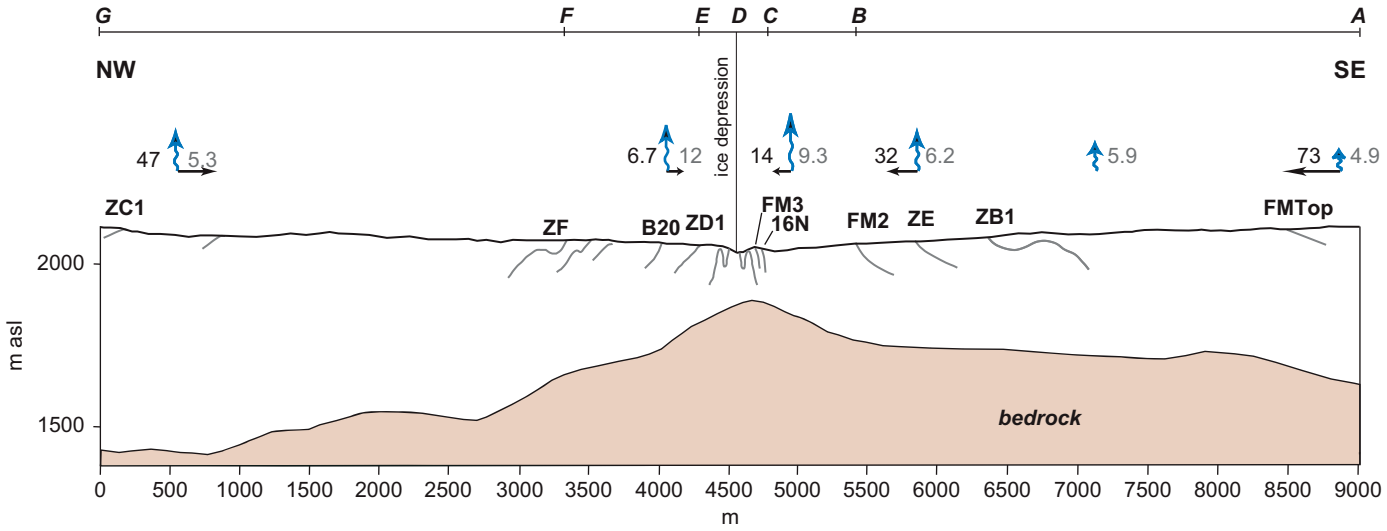

Fig. 4. Representative cross-section of the Frontier Mountain blue-ice field. Bedrock topography, ice thickness, ice velocities (horizontal arrows; in cm yr^{-1}) and ablation rates (vertical arrows; in cm yr^{-1}) are from Folco et al. (2002). Surface morphology is from Zeoli (2002). A 2 × vertical exaggeration is used. Note that the A–G scale (top) represents segments used for thickness estimates (see text and Fig. 3).

a succession of 20–30 bands within a ~200 m long stretch of the ice field (Figs. 2a and 3). The outcrops of the richest layers may be marked by a centimetric morphological depression, since the lower albedo of the dust-laden ice enhances sublimation.

Fig. 3 shows major tephra layers in the field. The outcrops of individual tephra layers typically extend laterally for up to some kilometers on both the southern and northern ice slopes, outlining two up-glacier concave patterns on the opposite flanks of the ice valley. In places, ample folds of the scale of tens of meters resulting from the intersection of undulated layers with the topographic surface occur. Decameter-scale folds with serrate hinges documenting stronger deformation are observed close to the bedrock (i.e., at the foot of the mountain and close to the small outcrop on the eastern side of the ice field) and at the bottom of the ice valley where the southern and northern ice flows meet.

Combining surface topography (Zeoli, 2002), bedrock topography and ice thickness (Folco et al., 2002) with the position and bedding of the tephra layers (Table 1), we reconstructed a representative cross-section of the Frontier Mountain blue-ice field (Fig. 4). The section extends to ~9 km from the northern to the southern edge of the blue-ice field across the ice valley, in a roughly northwest–southeast direction. Englacial tephra layers on the southern slope show S-dipping bedding (i.e., ice layers dip up-glacier) with increasing dip angles moving towards the ice depression. Undulations of the layers occur half-way along the section, whereas severe folding occurs in the ice depression. On the whole, the geometry of tephra layers thus describes an up-glacier, SE-dipping homocline. A similar structure is inferred for the northern ice flow, obviously with N-dipping bedding. The overall structure of each of the two ice bodies matches that predicted by the ice flow models for blue-ice fields (Naruse and Hashimoto, 1982; Whillans and Cassidy, 1983). In these models the age of the layers increases from the up-glacier to the down-glacier margin of the blue-ice area, where prolonged ablation has exhumed deeper, and thus older, ice. At Frontier Mountain, therefore, the layers cropping out at the valley bottom, i.e., where the fronts of the two ice flows meet, are the oldest ones, while the up-glacier layers should have increasingly younger ages.

Based on the cross-section shown in Fig. 4, we estimate the stratigraphic thickness of the Frontier Mountain blue ice. The southern ice flow consists of three portions: the 3500 m long AB segment, where layers have a median dip angle of 10°, the 750 m long BC segment, where layers have a median dip angle of 35°, and the 250 m long CD segment, which is characterized by almost vertical, severely folded layers. The stratigraphic thickness of the bulk of the southern ice flow calculated along the AC unfolded segment is therefore ~1000 m. The exercise can be repeated for the northern ice flow. The deformed DE segment measures ~250 m; the median dip angle is ~35° in the ~1050 m long EF segment, and 10° in the ~3200 FG segment. As a result, the estimated stratigraphic thickness of the bulk of the northern ice flow is ~1150 m.

4.2. Particle mineralogy and morphology

Most of the tephra were light brown to light gray, but a few (FMTop, ZA2, ZC1 and ZC1bis) stood out as markedly black. Tephra particles are <200 μm in diameter. All the specimens appear to consist exclusively of glass and igneous minerals with no contribution from the local country rocks. Glass is the major component of all the tephra layers; common minerals are ubiquitous igneous feldspars, variable clinopyroxenes and amphiboles, minor olivine, biotite, quartz and iron oxides. All these mineral phases occur as either individual particles or polymineralic

Table 2
Morphometrical parameter values (and, in brackets, standard deviations in the last digits) for the Frontier Mountain tephra derived from digital image analyses of polished sections

Sample	Number of analyzed particles	Average area (μm^2)	Maximal area (μm^2)	Average. perimeter (μm)	Average length (μm)	Average width (μm)	Maximal average radius (μm)	Minimal average radius (μm)	Average radius ratio	Five maximum area (μm^2)
ZA2	332	266 (432)	4633	72 (100)	23 (22)	13 (12)	13 (13)	3 (2)	9 (25)	2563
ZC1	280	922 (1208)	8390	114 (100)	41 (31)	24 (19)	23 (17)	7 (6)	6 (13)	6128
ZC1bis	1034	862 (1099)	9266	118 (100)	41 (29)	24 (18)	23 (16)	6 (5)	6 (15)	7532
FM Top	306	997 (1064)	6974	124 (97)	46 (32)	26 (18)	25 (18)	7 (6)	7 (14)	4889
FM3	1464	669 (1586)	33,042	90 (119)	30 (40)	18 (20)	17 (18)	4 (5)	7 (12)	17,857
B20	2571	758 (1668)	21,617	88 (110)	31 (33)	18 (20)	17 (18)	4 (6)	6 (8)	18,215
FM2	268	474 (563)	4558	93 (83)	32 (23)	19 (14)	18 (13)	4 (4)	6 (8)	2983
ZF	2631	57 (145)	2548	27 (32)	10 (9)	5 (5)	5 (5)	1 (1)	7 (10)	1792
ZE	2109	78 (171)	1753	33 (39)	12 (11)	6 (6)	7 (6)	1 (1)	8 (11)	1460
ZA8	282	1330 (1583)	7600	165 (159)	50 (39)	31 (25)	28 (22)	7 (7)	9 (16)	6606
ZA1	250	1458 (1313)	6966	157 (114)	54 (33)	32 (21)	29 (18)	9 (7)	6 (9)	5644
ZA4	844	20 (38)	724	15 (19)	6 (6)	3 (3)	3 (3)	1 (1)	5 (7)	349
16S	4415	94 (221)	2300	34 (39)	12 (12)	7 (7)	7 (6)	2 (2)	6 (9)	2123
ZD1	323	2354 (3550)	26,532	189 (186)	64 (55)	38 (32)	35 (30)	9 (9)	9 (25)	19,323
ZA3	559	1842 (2780)	23,280	171 (185)	59 (50)	34 (29)	33 (27)	7 (7)	8 (12)	16,985
B1	903	159 (354)	5495	47 (63)	16 (16)	9 (9)	9 (9)	2 (2)	7 (14)	3234
FM1	469	364 (844)	9168	76 (120)	23 (26)	14 (16)	13 (14)	3 (3)	9 (24)	6175
B16	688	57 (79)	963	27 (28)	10 (10)	6 (4)	6 (5)	2 (1)	5 (9)	620
B19	693	246 (284)	2472	70 (62)	25 (17)	13 (9)	14 (10)	3 (2)	10 (24)	2022
B17	633	321 (404)	3949	75 (71)	27 (20)	15 (11)	15 (11)	3 (2)	8 (13)	2868
ZB1	429	402 (493)	3750	75 (66)	27 (20)	16 (11)	15 (11)	4 (3)	6 (10)	3001
ZA9	228	1052 (1427)	11,599	132 (143)	48 (44)	26 (20)	26 (23)	6 (4)	8 (16)	7466

Note that, due to sectioning, morphometrical parameters are underestimated.

lithic fragments. The glass shards of layers B19 and B20 also contain blebs of a more primitive, glass up to 100 μm in apparent size, providing evidence of magma mingling. Glass is vesicular and characterized by delicate cuspate shapes. It shows no evidence of abrasion, mechanical reworking or weathering, all of which are characteristics of an unmodified air fall deposit. The color of individual shards is variable, from transparent brown with minor dark opaque zones to yellow-gray. Fragments whiten with increasing amounts of vesicles.

The average particle size ranges from 4 to 5 μm to more than 100 μm, with typical values close to 40 μm (Table 2). Size-sorting is moderate within individual samples, but size contrast is evident from sample to sample. In the different samples, the number of analyzed particles ranges from 228 to 4506. Particle sizes vary considerably from one layer to another (Table 2). In particular, the average perimeter and average area span over one–two orders of magnitude; we thus considered these to be the most significant morphometric parameters (Fig. 5).

4.3. Chemical compositions of the glass shards

The major element compositions of glass shards are reported in Table 3. Individual shards have fairly homogeneous compositions, as indicated by the low deviations from the averages. Based on the total alkali-silica classification scheme (Le Bas et al., 1986), the shards from the ZA2, FMTop, ZC1 and ZC1bis layers have tephritic (olivine normative <10 vol%) compositions, those from the ZA8 layer have phonolitic compositions, and those from all other layers have trachytic compositions (Fig. 6a). The primitive glass seldom found associated with the trachytic glass (see Section 4.2) in B19 and B20 has a tephritic composition. All samples fall within the field for alkaline rocks (Fig. 6a). The $(Na_2O–2)/K_2O$ weight ratios are typically in the normal 0.6–0.9 range, whereas values of 1.1 are observed in B1, ZA2, ZA8 and FMTop, denoting a weak sodic character. The agpaitic index, i.e., the molecular $(Na_2O+K_2O)/Al_2O_3$ ratio, is generally $\leqslant 1$, although samples B1 and ZB1 have a weak peralkaline character with values of 1.19 and 1.08, respectively (Fig. 6e).

Table 4 lists the trace element compositions of the FM2, FM3, B19 and B20 trachytic glasses and of the coexisting B19 and B20 tephritic glasses. Fig. 7a shows the chondrite-normalized rare-earth element (REE) distributions for the FM2, FM3, B19 and B20 trachytic glasses. FM2, FM3 and B20 show very similar, nearly smooth patterns characterized by moderately fractionated light rare-earth element (LREE), with La_N/Sm_N ranging from 5.7 to 9.6, weakly fractionated heavy rare-earth element (HREE), with Gd_N/Lu_N ranging from 1.4 to 2.2, and minor europium anomalies in the 0.6–1.1 Eu/Eu* range. Glass B19 shows a slightly different pattern. Major differences include a less fractionated REE pattern ($La_N/Lu_N = 13.3$), mainly due to higher HREE concentrations, and a significant negative europium anomaly Eu/Eu* = 0.3. In addition, B19 shows very low Sr and Ba

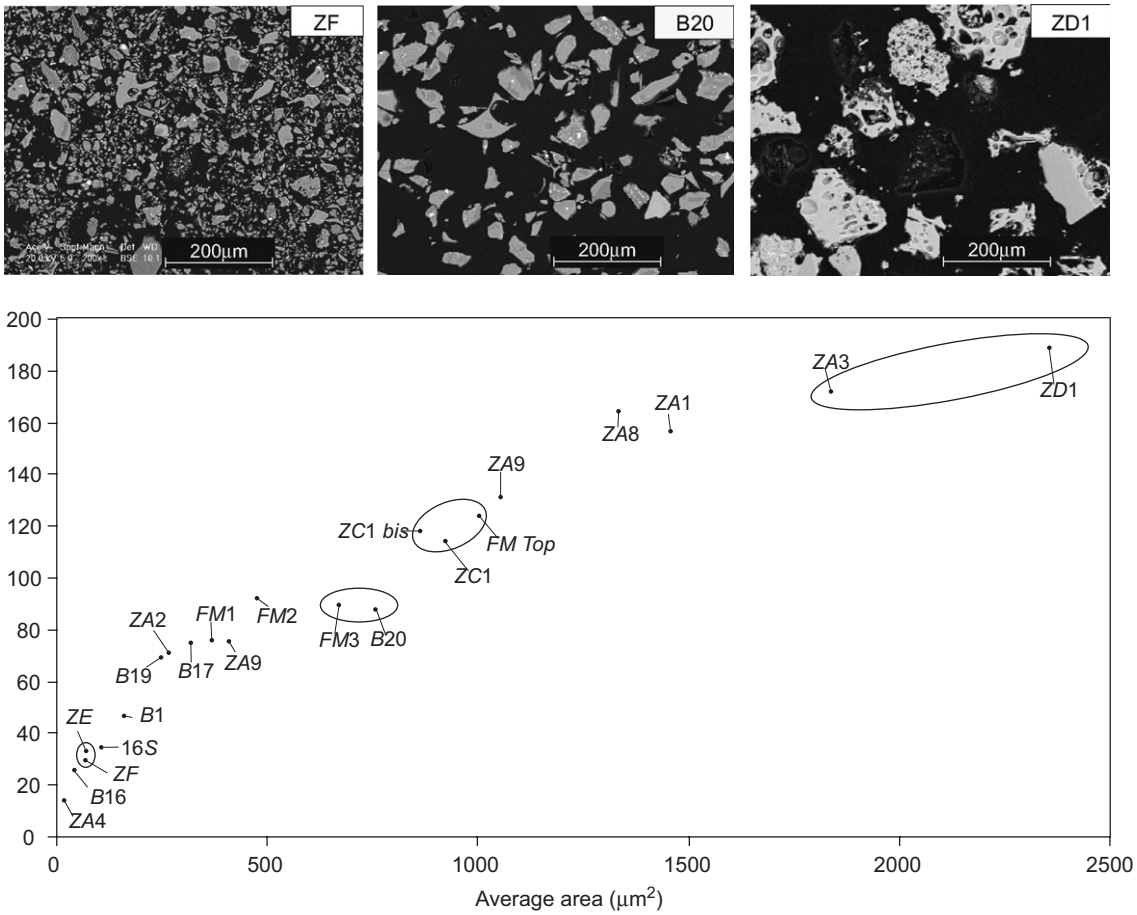

Fig. 5. Average area versus average perimeter plot derived from image analysis, and backscattered electron images of selected samples.

concentrations (19 and 240 ppm, respectively). These features coupled with the relatively higher silica content, suggest that B19 represents a more evolved liquid which experienced greater feldspars fractionation.

Tephritic glasses B19 and B20 have very similar trace element concentrations. They are characterized by nearly rectilinear chondrite-normalized REE distributions with no significant europium anomalies ($Eu/Eu^* = 0.9$ and 1.0 in B19 and B20, respectively), LREE enrichment ($La_N = 273$ and 323), and similar REE fractionation ($La_N/Lu_N = 22.4$ and 19.6). Fig. 7b shows their overall primitive mantle normalized distribution of incompatible elements. Both B19 and B20 are characterized by modest ratios Nb–Ta to large ion lithophile elements (LILE, e.g., Rb, Ba, Th, and U) and Y-HREE.

4.4. Bulk chemical compositions

Bulk chemical compositions of tephra layers are reported in Table 5, together with three sets of data previously obtained on pressed pellets (FM1, FM2 and FM3; Perchiazzi et al., 1999). Data are normalized to 100 wt%, on an anhydrous base and all the iron is expressed as ferrous iron.

Layers ZA2, ZC1, ZC1bis and FMTop have basaltic to tephritic compositions, whereas the others range from trachyandesites to trachytes (Fig. 6b). All layers typically show an alkaline character (Fig. 6b), similar to that observed in the glass shards.

Trace element concentrations follow the patterns already described by Perchiazzi et al. (1999). Strontium and barium (Table 4) are negatively correlated with silica, rubidium, yttrium, niobium and zirconium, and rare-earth lanthanum and cerium, thus revealing defined differentiation trends. These are evident in the spider diagrams of Fig. 8, where samples are shown in order of increasing silica content. The different trace element signatures therefore provide us with a further tool for identifying pairs of tephra layers unrelated in the field.

4.5. ^{40}Ar–^{39}Ar dating

^{40}Ar–^{39}Ar analyses of the 16S and ZD1 tephra layers yielded reliable geochronological data. Five step-heating analyses were performed on aliquots of the 16S glass separates and four gave plateau ages overlapping at the 2σ level (Table 6). The spread in plateau ages is high but similar to that obtained from the analyses of separates of young lava flows with low radiogenic ^{40}Ar yields (Heizler et al., 1999). The weighted and simple average of plateau ages are 50.0 ± 17 ka (95% conf., mean square of weighted deviates,

Table 3
EMP major element composition (oxides wt% and, in brackets, standard deviations in the last digits) of glass shards from Frontier Mountain tephra layers

	ZA2 ($n = 8$)	FM Top ($n = 10$)	ZC1 ($n = 8$)	ZC1bis ($n = 19$)	FM2 ($n = 10$)	ZA8 ($n = 8$)	ZF ($n = 18$)	ZE ($n = 21$)
SiO_2	42.9 (8)	45.2 (1)	45.7 (10)	46.3 (2)	59.0 (4)	59.2 (3)	59.4 (2)	59.5 (17)
TiO_2	3.63 (8)	3.69 (36)	3.47 (14)	3.59 (31)	0.94 (9)	0.28 (1)	0.85 (23)	0.76 (17)
Al_2O_3	15.5 (3)	15.8 (4)	15.2 (6)	15.7 (3)	17.4 (3)	19.4 (2)	17.7 (5)	17.8 (4)
FeO	11.2 (4)	11.4 (2)	11.2 (3)	11.4 (4)	6.92 (4)	3.93 (5)	6.26 (94)	6.01 (80)
MnO	0.21 (5)	0.20 (3)	0.20 (6)	0.22 (4)	0.24 (4)	0.23 (3)	0.23 (5)	0.20 (4)
MgO	5.15 (22)	4.74 (52)	3.91 (21)	4.25 (58)	0.99 (13)	0.14(3)	0.84 (31)	0.77 (27)
CaO	11.0 (0)	10.3 (13)	8.9 (1)	9.18 (115)	2.82 (19)	1.62 (25)	2.27 (50)	2.11 (39)
Na_2O	4.08 (38)	4.19 (33)	4.39 (42)	4.68 (41)	5.92 (16)	7.99 (27)	6.4 (4)	6.23 (47)
K_2O	2.03 (7)	2.08 (44)	2.41 (6)	2.32 (29)	4.99 (26)	5.54 (13)	5.06 (31)	5.13 (31)
F	0.22 (5)	0.12 (7)	0.16 (5)	0.2 (9)	0.16 (10)	0.04 (3)	0.2 (1)	0.16 (13)
Cl	0.11 (1)	0.08 (2)	0.12 (1)	0.11 (1)	0.16 (1)	0.4 (1)	0.17 (1)	0.18 (2)
P_2O_5	1.23 (3)	0.85 (11)	1.16 (10)	1.2 (19)		0.19 (21)	0.32 (13)	0.23 (9)
Sum	97.3	98.8	96.9	99.2	99.6	98.9	99.7	99.1
	ZA1 ($n = 9$)	ZA4 ($n = 8$)	B20 (Trachytic) ($n = 11$)	B20 (Tephritic) ($n = 1$)	FM3 ($n = 10$)	ZD1 ($n = 9$)	ZA3 ($n = 7$)	16S ($n = 13$)
SiO_2	59.7 (19)	61.0 (15)	61.1 (18)	45.8	61.3 (9)	61.7 (11)	62.1 (6)	62.4 (10)
TiO_2	0.28 (8)	0.38 (17)	0.53 (9)	3.35	0.34 (7)	0.41 (6)	0.36 (7)	0.4 (4)
Al_2O_3	17.7 (5)	17.4 (3)	17.8 (11)	17.7	17.2 (4)	17.5 (2)	17.5 (3)	17.6 (3)
FeO	5.45 (60)	5.79 (22)	4.30 (64)	11.6	3.50 (34)	4.90 (8)	4.86 (38)	4.51 (21)
MnO	0.25 (4)	0.24 (2)	0.14 (3)	0.31	0.14 (5)	0.16 (5)	0.20 (3)	0.16 (3)
MgO	0.36 (4)	0.20 (16)	0.56 (17)	4.21	0.31 (11)	0.22 (7)	0.17 (8)	0.33 (2)
CaO	1.38 (32)	1.26 (42)	1.79 (28)	10.5	1.44 (17)	1.24 (18)	1.14 (12)	1.46 (9)
Na_2O	6.48 (100)	6.62 (57)	6.07 (38)	3.2	6.31 (24)	5.91 (56)	6.20 (20)	6.35 (24)
K_2O	5.38 (69)	5.01 (17)	4.94 (27)	2.8	5.22 (16)	5.50 (17)	5.46 (22)	5.50 (13)
F	0.09 (10)	0.25 (12)				0.16 (8)	0.20 (4)	0.12 (9)
Cl	0.57 (9)	0.23 (4)			0.17 (4)	0.19 (2)	0.23 (6)	0.26 (2)
P_2O_5	0.29 (28)	0.06 (7)						0.1 (6)
Sum	97.9	98.4	97.2	99.5	95.9	97.9	98.4	99.2
	B1 ($n = 5$)	ZB1 ($n = 7$)	B16 ($n = 4$)	FM1 ($n = 10$)	B19 (Trachytic) ($n = 7$)	B19 (Tephritic) ($n = 2$)	B17 ($n = 6$)	ZA9 ($n = 9$)
SiO_2	62.5 (2)	63.3 (19)	63.3 (5)	63.6 (9)	66.1 (18)	43.9	66.3 (7)	66.6 (15)
TiO_2	0.49 (41)	0.25 (7)	0.29 (112)	0.22 (3)	0.25 (9)	3.5	0.26 (5)	0.2 (4)
Al_2O_3	12.9 (5)	13.6 (9)	17.0 (13)	15.5 (12)	15.3 (6)	16.3	15.4 (3)	14.8 (10)
FeO	7.42 (58)	6.65 (89)	4.64 (47)	6.33 (132)	4.64 (91)	11.7	4.81 (54)	3.84 (57)
MnO	0.43 (2)	0.32 (11)	0.21 (9)	0.33 (9)	0.19 (4)	0.17	0.17 (2)	0.13 (4)
MgO	0.03 (0)	0.04 (3)	0.29 (4)		0.01 (1)	5.22	0.02 (1)	
CaO	1.18 (23)	1.09 (15)	1.58 (40)	1.03 (28)	1.08 (41)	11.7	1.25 (21)	0.83 (30)
Na_2O	6.53 (24)	5.90 (132)	6.03 (11)	6.44 (19)	4.97 (88)	4.42	5.41 (21)	5.89 (20)
K_2O	4.32 (0)	4.67 (56)	5.12 (75)	4.72 (11)	4.88 (41)	2.08	5.08 (18)	4.92 (47)
F		0.73 (25)		0.59 (22)				0.23 (8)
Cl		1.06 (9)		0.8 (3)				0.41 (3)
P_2O_5		0.09 (12)						
Sum	95.8	97.7	98.4	99.5	97.4	99.0	98.7	97.9

n = number of analyses.

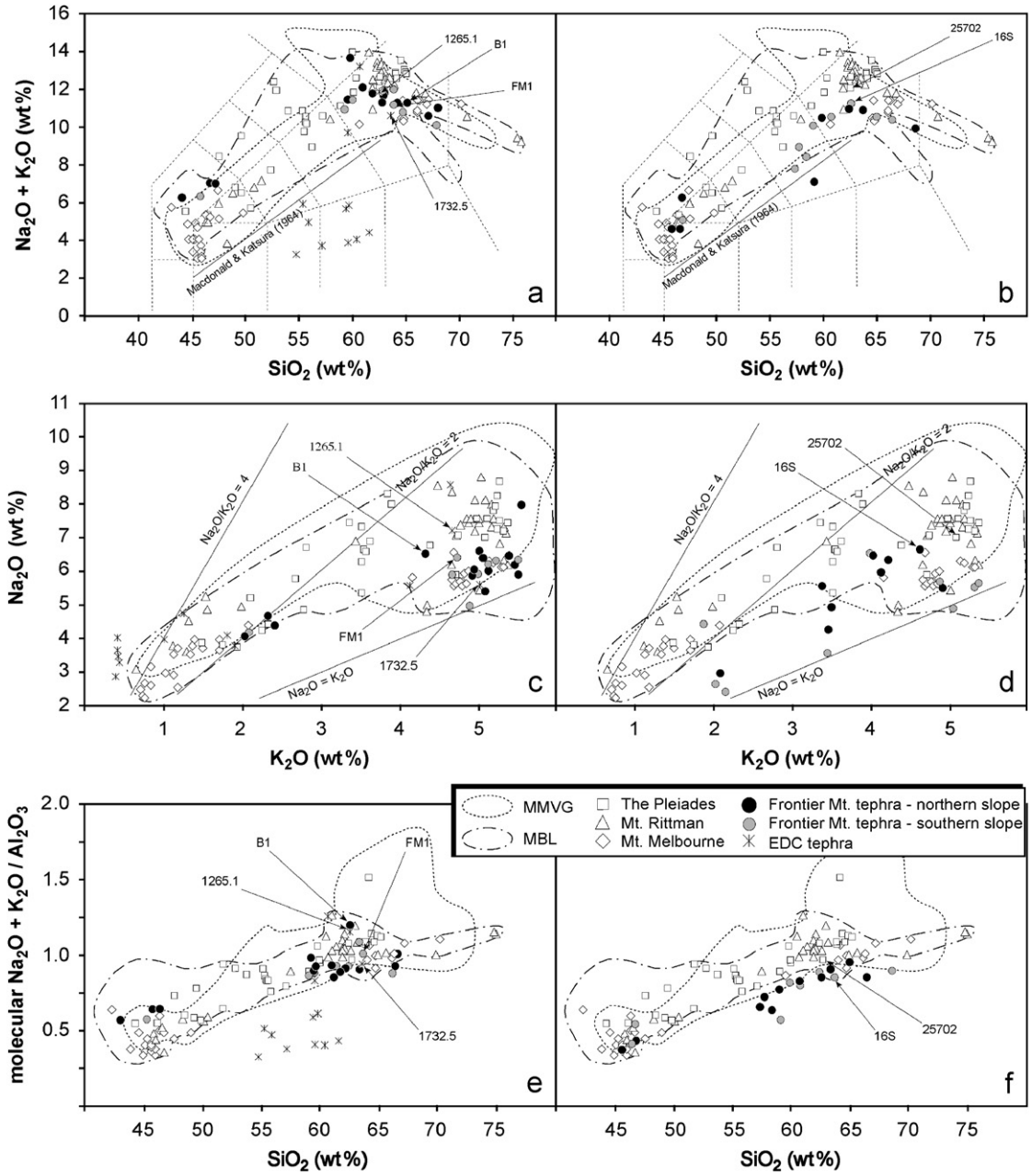

Fig. 6. (a) Total alkali versus silica diagram for the glass shards from the Frontier Mountain tephra layers. IUGS classification boundaries (Le Bas et al., 1986) are shown by dashed lines. The alkaline/subalkaline field boundary (Macdonald and Katsura, 1964) is shown by a solid line. (b) The same diagram for the bulk samples. (c) K_2O versus Na_2O diagram for the glass shards from the Frontier Mountain tephra layers. (d) The same diagram for the bulk sample. (e) Molecular $(Na_2O+K_2O)/Al_2O_3$ versus silica diagram for the glass shards from the Frontier Mountain tephra layers. (f) The same diagram for the bulk sample. Literature compositional data for rocks from the McMurdo Volcanic Group (MMVG) and Marie Byrd Land (MBL) volcanic provinces, The Pleiades, Mount Rittman and Mount Melbourne volcanoes, and the glass shards from the EPICA-Dome C tephra layers (EDC) are shown for comparison. Data sources: the compositional fields for the MMVG and MBL volcanic provinces in (a) and (b) were redrawn from LeMasurier and Thomson (1990); the compositional field for MMVG shown in (c)–(f) was obtained from 185 rock analyses listed in LeMasurier and Thomson (1990), Armienti and Tripodo (1991), Kyle (1982), Wörner et al. (1989); the compositional field for MBL shown in (c)–(f) was obtained from 68 rock analyses listed in LeMasurier and Rex (1989, 1991); data points for The Pleiades, Mount Rittman and Mt. Melbourne volcanic rocks are from Armienti and Tripodo (1991), Kyle (1982) and Wörner et al. (1989); data points for the EPICA-Dome C glass shards are from Narcisi et al. (2005). Arrowed data points refer to samples individually discussed in Section 5.

MSWD = 1.9) and 48.8 ± 10 ka, respectively (Table 6). The points that concur to the plateau ages (Table SM1) define an isochron age of 49 ± 11 ka (95% conf., MSWD = 1.01) with an atmospheric initial ratio (Fig. 9a).

Eight step-heating experiments of several aliquots of the ZD1 leached feldspathic fraction produced age spectra with different shapes, and six of them gave plateau ages (Table 6) with a weighted and simple average of

Table 4
LM–ICP–MS trace element compositions (ppm) of selected glass shards

	FM2 (trachytic)	FM3 (trachytic)	B19 (trachytic)	B19 (tephritic)	B20 (trachytic)	B20 (tephritic)
Rb	102	201	161	60	244	61
Sr	398	238	19	798	319	1105
Y	24	27	58	30	26	26
Zr	314	635	997	267	806	266
Nb	102	165	156	76	142	93
Cs	1.6	4.9	2.0	0.6	5.0	0.5
Ba	977	771	240	464	813	648
La	73	106	128	64	114	76
Ce	122	190	218	124	179	133
Pr	12.7	16.1	20.2	13.7	15.9	13.2
Nd	49.3	52.9	87.6	67.4	54.9	64.3
Sm	8.0	6.87	19.1	10.2	8.1	11.4
Eu	2.4	1.2	1.6	2.5	1.6	3.4
Gd	6.0	5.1	14.2	7.1	7.1	9.8
Tb	1.07	0.72	2.12	1.41	0.87	1.17
Dy	4.6	4.7	16.6	10.0	5.4	7.2
Ho	0.95	1.06	2.18	1.48	0.87	1.23
Er	2.7	2.5	7.2	3.8	3.0	2.7
Tm	0.33	0.52	0.94	0.45	0.51	0.23
Yb	2.9	3.6	7.3	3.6	3.3	3.5
Lu	0.33	0.45	1.00	0.30	0.54	0.40
Hf	7.2	12.3	20.1	6.8	17.2	5.9
Ta	5.4	11.1	7.9	3.9	8.8	5.1
Pb	10.7	20.7	15.8	5.8	18.6	3.8
Th	9.0	28.1	19.4	8.2	29.3	6.8
U	2.25	7.93	4.75	2.20	8.17	1.82
Eu/Eu^*[a]	1.1	0.6	0.3	0.9	0.6	1.0
La_N/Sm_N	5.7	9.6	4.2	3.9	8.8	4.2
Gd_N/Lu_N	2.2	1.4	1.8	3.0	1.6	3.0
La_N/Lu_N	22.6	24.2	13.3	22.4	21.9	19.6

[a] $Eu/Eu^* = Eu_N/\sqrt{Gd_N * Sm_N}$.

98.3 ± 8.3 ka (95% conf., MSWD = 1.5) and 98.2 ± 7.4 ka (1σ), respectively. The points that form the plateaus of individual experiments identify an isochron age of 100.2 ± 5.3 ka (95% conf., MSWD = 1.31; Fig. 9b) with an atmospheric trapped component.

The other analyzed tephra layers, ZC1bis, ZE, B20, FM3 and FMTop, did not produced reliable ages due to (i) undetectable amounts of radiogenic ^{40}Ar from high background levels of trapped atmospheric ^{40}Ar, or to (ii) the presence of extraneous ^{40}Ar. The reader is referred to the Supplementary Material for a detailed description and interpretation of experimental data.

5. Discussion

5.1. Chronostratigraphy

Mineralogical, geochemical and morphometrical data define each of the tephra layers cropping out on the northern and southern slopes of the Frontier Mountain blue-ice field, thereby enabling detailed ice stratigraphy. For instance, undisturbed or duplicate (e.g., folded and thrusted) successions may be identified. The lateral continuity of a layer may be checked when masked by seasonal snow cover or interrupted by a structural discontinuity. Moreover, correlations between layers of the two ice flows of the Frontier Mountain blue-ice field, which are derived from adjacent snow accumulation areas (Fig. 1) become possible. For instance, the identical ZD1 and ZA3 samples are from a single layer cropping out on the northern slope for ~4 km, all along the foot of the mountain to the bottom of the ice valley (Fig. 3). ZC1 and ZC1bis are duplicate samples collected a few meters apart from a layer cropping out at the northern margin of the blue-ice field (Fig. 3). The indistinguishable mineralogical, geochemical and morphometrical features of these two pairs of samples (Tables 2–4) demonstrate the validity of the adopted approach. Similarly, the B-series, on the northern slope, comprises two correlated tephra (B17 and B19), interpreted as evidence of a local fold in the B sequence which could not be detected in the field. Conversely, samples B17 and ZA9, as well as samples ZC1 and ZA2, show similar geochemical features (Table 5), but their different particle sizes (Table 2) precludes the possibility that they were produced during the same eruption. Likewise, although samples 16N and FMM from the southern ice flow, have similar geochemical compositions, their distinct morphometrical features suggest that they are unrelated.

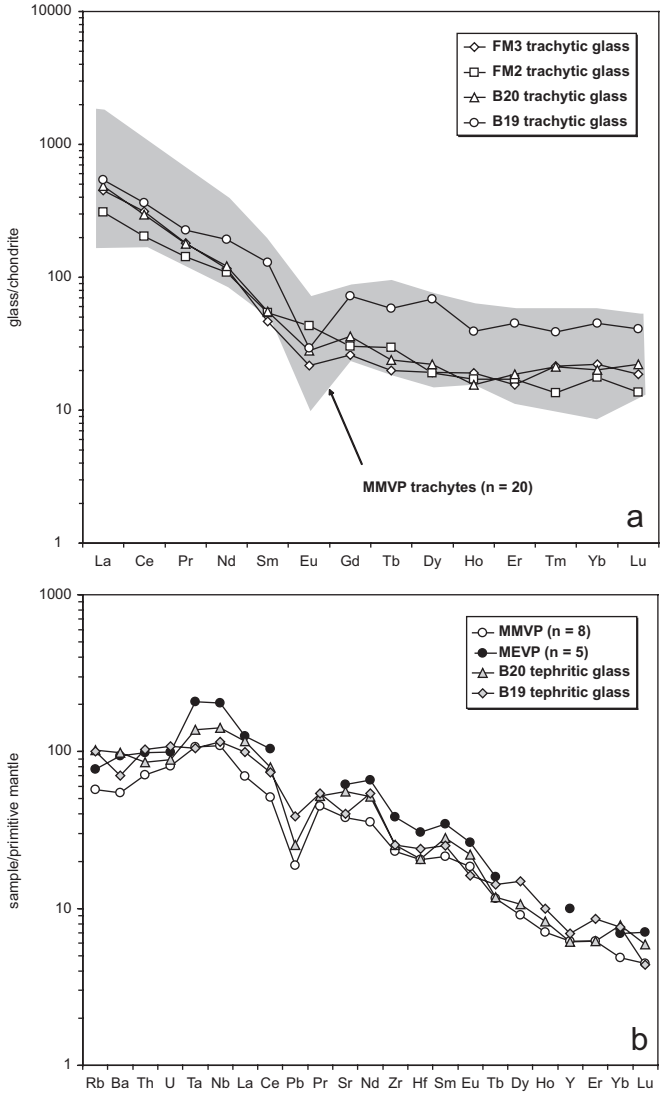

Fig. 7. (a) Chondrite normalized (McDonough and Sun, 1995) rare earth element spidergram for selected evolved glass shards from Frontier Mountain tephra layers. The shaded compositional field refers to Mount Melbourne Volcanic Province trachytes ($n = 20$; Kyle and Rankin, 1976; Wörner et al., 1989; S. Rocchi and M. D'Orazio, 2007, pers. comm.) of the McMurdo Volcanic Group, MMVG. (b) Primitive mantle normalized (McDonough and Sun, 1995) multielement spidergram of selected glasses of tephritic compositions from Frontier Mountain tephra layers. Averages of Mount Melbourne Volcanic Province (MMVP) and Mount Erebus Volcanic Province (MEVP) mafic rocks from Rocchi et al. (2002) are plotted for comparison.

Three pairs of layers from the northern and the southern slopes are correlated, because they show overlapping morphometrical parameters (Table 2) and geochemical composition (Tables 3 and 5). Layers ZC1 and FMTop crop out at the top of the two slopes (Figs. 3 and 4). In the field, they appear as the thickest and darkest layers of the whole ice field. Layers ZE and ZF crop out half-way down the ice slopes (Figs. 3 and 4). They are amongst the most fine-grained samples. FM3 and B20 form the third pair of correlated layers. FM3 crops out on the southern slope close to the ice valley bottom, and B20 on the northern slope, ~750 m uphill from the bottom of the ice valley.

Based upon these correlations and the structural reconstruction presented in Section 4.1, we derived the correlation chart for the Frontier Mountain blue ice reported in Fig. 10 which accounts for ~1150 m in thickness. As shown by the two stratigraphic columns of the southern and northern ice flows, the FMTop–ZC1 layer marks the top of the succession. The layers belonging to the ZA-series mark the bottom of the succession. Although the B-series might be correlated to the ZA-series on the basis of our geometric reconstruction, additional sampling is required to confirm this finding. The dating of the ZD1 and 16S tephra layers constrains the age of the ice succession cropping out at Frontier Mountain. The ZA–ZD1 layer with an ^{40}Ar–^{39}Ar age of 100 ± 5 ka (Fig. 9b) indicates that the ~1150 m thick ice succession has a maximum age of ~100 ka. The 16S layer has an ^{40}Ar–^{39}Ar age of 49 ± 11 ka (Fig. 9a). This layer thus shows that the upper ~950 m of the ice succession are younger than 49 ± 11 ka. Since the 16S layer lies close to the FM3–B20 stratigraphic level, this portion of the ice succession, with an age up to ~50 ka, constitutes nearly all of the ice under ablation on the southern slope and about 90% of the ice under ablation on the northern slope (Fig. 4). Note that our age–depth results for the Frontier Mountain blue ice agree well with the age–depth profiles calculated for the Talos Dome ice core, which predict that 50 and 100 ka-old layers should lie at depths between 900 and 1400 m, and between 1110 and 1600 m, respectively (Deponti and Maggi, 2002; Frezzotti et al., 2004). In addition, our estimate of the age of the ice under ablation on the southern slope agrees with that inferred by Folco et al. (2006) on the basis of the terrestrial age (the time since their fall) of the meteorites found there.

5.2. Source volcanoes

By combining data on particle size, glass and bulk chemical compositions, and age estimates, we are able to constrain the source of the Frontier Mountain tephra, following Perchiazzi et al. (1999).

Volcanic ashes may undergo either stratospheric or tropospheric transport; their source may thus be either remote or proximal, respectively. Particle size distributions of tephra allow the distinction between the two transport mechanisms (Lisitzin, 1996) and limit the distance from the source. While tropospheric ash fallout is dominated by particles in the 10–50 μm size range, stratospheric ash fallout consists of mechanically sorted fine dust, with a median diameter below 1 μm and rare particles larger than 3–5 μm. As the particle radii of the Frontier Mountain ashes are typically up to tens of micrometers (Table 2), deposition occurred after tropospheric transport.

In the case of tropospheric transport, particle size also provides information on the distance from the eruptive center, with size decreasing with distance (Lisitzin, 1996).

Table 5
XRF major (wt%) and trace element (ppm) bulk composition of tephra layers from Frontier Mountain

	ZA2	ZC1	ZC1 bis	FM Top	FM3	16N	FMM	FM2	B20	ZF	ZE	ZA8	ZA4	16S	ZD1	ZA3	FM1	ZB1	ZA9
SiO_2	45.8	46.5	46.7	46.8	57.4	57.7	58.4	59.0	59.1	59.9	60.7	60.8	62.6	62.6	63.7	64.1	65.0	66.5	68.6
TiO_2	3.48	3.66	3.17	3.64	1.64	1.46	1.19	1.11	1.46	0.82	0.70	0.68	0.54	0.49	0.50	0.44	0.49	0.28	0.28
Al_2O_3	16.1	15.8	17.1	16.6	16.4	17.7	18.7	18.4	16.7	18.4	18.2	18.2	16.9	18.6	17.5	17.2	15.7	16.8	15.1
FeO	12.0	12.4	10.6	12.0	7.91	6.95	6.54	7.1	7.39	6.27	6.01	5.72	6.85	4.57	5.28	5.12	4.88	4.14	4.76
MnO	0.20	0.19	0.18	0.19	0.18	0.16	0.16		0.17	0.19	0.18	0.20	0.20	0.14	0.17	0.17	0.15	0.16	0.15
MgO	5.58	6.22	6.31	5.27	3.13	2.7	2.79	0.61	2.68	1.07	0.96	0.92	0.50	0.41	0.48	0.27	1.34	0.43	0.02
CaO	11.1	9.76	8.71	9.73	5.29	3.98	3.52	3.64	5.07	2.54	2.40	2.78	1.48	1.73	1.45	1.38	1.75	1.24	1.10
Na_2O	2.41	2.65	4.42	2.99	4.27	5.58	4.93	5.96	3.56	6.53	6.51	5.68	5.63	6.65	5.55	5.87	6.34	5.52	4.90
K_2O	2.16	2.03	1.88	2.09	3.45	3.38	3.49	4.14	3.45	4.02	4.03	4.86	5.36	4.63	5.33	5.34	4.22	4.90	5.06
P_2O_5	1.12	0.81	0.85	0.70	0.40	0.34	0.32	–	0.41	0.27	0.29	0.14	0.09	0.12	0.05	0.04	0.11	0.01	–
Co	44	44	41	44	21	22	20		25	16	16	15	15	12	11	10	10	9	10
Rb	44	42	41	46	127	99	116		116	106	111	200	142	170	130	146	299	335	221
Sr	812	742	717	770	581	413	393		574	325	310	377	77	200	56	58	96	48	11
Y	35	25	24	25	33	29	37		27	40	34	40	74	32	69	68	64	75	114
Zr	250	201	208	217	468	465	448		433	574	593	817	887	815	810	898	955	1165	1363
Nb	110	86	92	87	132	112	129		122	141	150	207	182	161	166	174	322	367	308
Ba	648	637	398	563	779	420	390		811	864	905	644	481	556	257	233	157	38	58
La	74	71	73	63	99	98	102		101	111	103	158	134	126	105	126	203	235	201
Ce	161	113	120	125	154	151	183		178	185	201	236	263	199	205	229	295	417	351

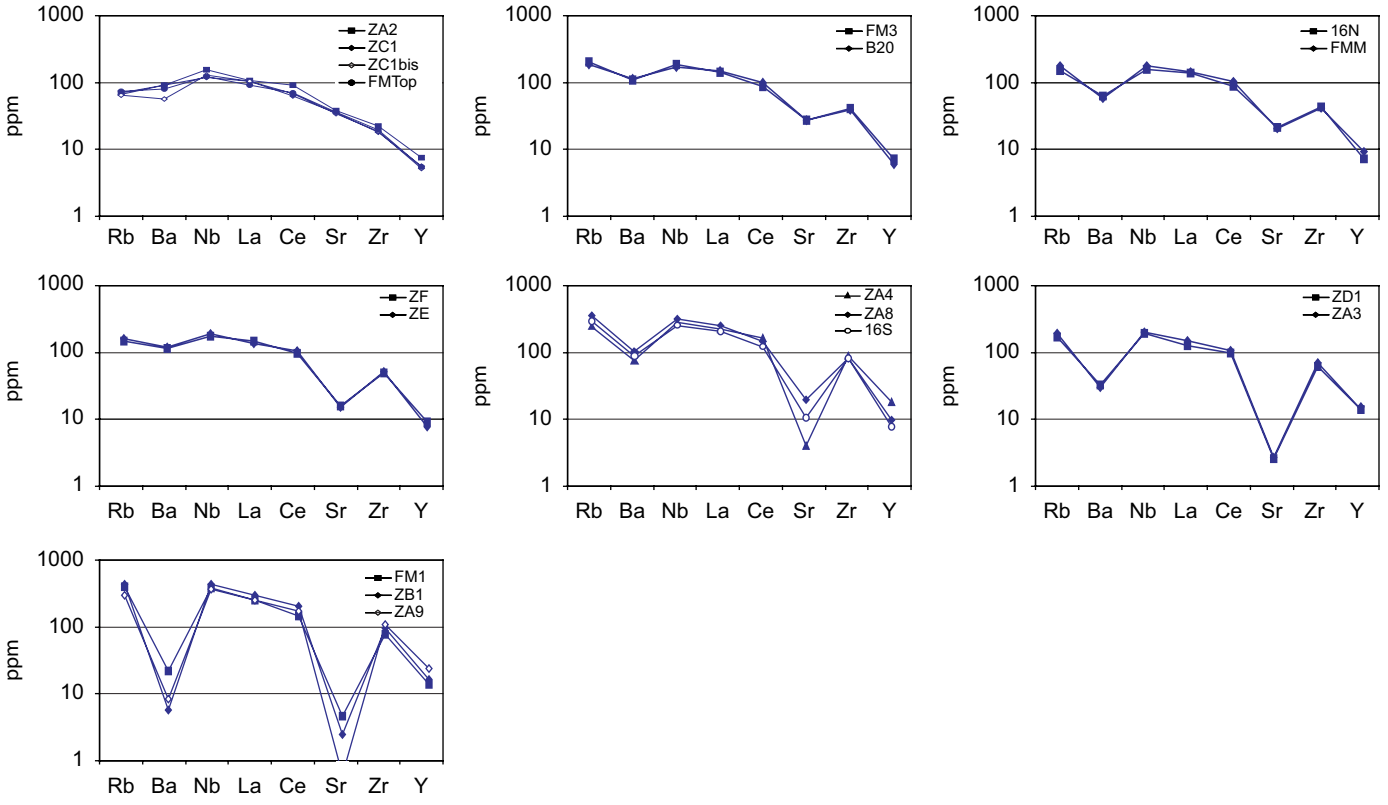

Fig. 8. Primitive mantle normalized (McDonough and Sun, 1995) multielement spidergrams of Frontier Mountain tephra layers.

Although variable wind regimes and outburst energies may account for some dispersion, this relation indicates an upper limit of ~1000 km for all the Frontier Mountain tephra layers. A proximal source is also supported by the presence of individual particles consisting of mafic minerals with high specific gravity (i.e., clinopyroxenes, amphiboles, olivine, and iron oxides), which are indicative of short-range transport (Juvigne and Porter, 1985; Lisitzin, 1996).

Volcanic ashes may also undergo selective sorting of mineral particles of contrasting specific gravity during atmospheric transport and deposition, and the resulting bulk composition may therefore not reflect the magmatic

Table 6
Summary table of the ^{40}Ar–^{39}Ar analyses performed on samples 16S (dark glass) and ZD1 (leached feldspathic fraction)

Analyses #	Plateau age (ka)	$\pm 1\sigma$	Steps	^{39}Ar %	MSWD	Total age (ka)	$\pm 1\sigma$	K/Ca	$\pm 1\sigma$
16S (dark glass)									
56#13-1	60.1	8.1	6	47	0.59	254	98	3.2	0.1
56#13-2	52.7	5.7	5	57	0.73	76	19	3.1	0.1
56#13-3	34.2	8.2	6	59	1.08	106	23	2.9	0.1
56#13-4						*176*	*76*	*2.7*	*0.2*
56#13-5	54.5	12.2	3	39	1.69	187	26	2.9	0.3
Simple average of plateau age ($\pm 1\sigma$): 48.8 ± 10 ka									
Weighted average of plateau age ($n = 4$): 50 ± 17 ka (95% conf.)									
ZD1 (feldspathic fraction)									
56#28-1						*489*	6	6.5	0.3
56#28-2	99.3	10.7	3	72	2.27	144	6	6.6	0.4
56#28-3	95.9	4.2	4	68	0.74	136	6	7.0	0.6
56#28-4	86.7	7.3	4	100	0.98	87	7	6.3	0.7
56#28-5						*106*	7	5.6	0.6
56#28-6	94.5	8.6	3	94	0.79	102	11	4.6	1.5
56#28-7	101.8	7.3	4	100	0.03	102	8	2.1	0.8
56#28-8	111	6.2	4	100	1.75	112	5	9.4	7.8
Simple average of plateau age ($\pm 1\sigma$): 98.2 ± 7.4 ka									
Weighted average of plateau age ($n = 6$): 98.3 ± 8.3 ka (95% conf.)									

Steps = number of contiguous steps used to calculate plateau ages.
^{39}Ar% = percentage of ^{39}Ar release pertinent to the plateau age.
MSWD = mean square weighted deviates.
Total age = age calculated from the sum of all radiogenic ^{40}Ar and K-derived ^{39}Ar (it is equivalent to a K/Ar age).
K/Ca = elemental ratio calculated from the whole analysis.
The analyses that did not produce plateau ages are in italics.

composition. The chemical composition of glass, instead, does represent magmatic fractionation. As such, the chemical composition of glass shards is a more reliable tool for tracing the parent magmatic province of englacial tephra layers (e.g., Nishio et al., 1985; Perchiazzi et al., 1999). The geochemical signatures of the glass shards and bulk samples of the Frontier Mountain tephra (Tables 2 and 3) compare closely with the majority of the active volcanic provinces of the Antarctic plate. In particular, their alkaline character matches the Cenozoic magmatism associated with the West Antarctic Rift System (WARS) (LeMasurier and Thomson, 1990)—one of the Earth's major active continental extension zones extending across the Antarctic continent for more than 3000 km from the western Ross Embayment to the Antarctic Peninsula (Behrendt et al., 1991). Both particle size and geochemistry thus indicate that the source for the Frontier Mountain tephra should be sought within the WARS intraplate volcanic provinces.

Frontier Mountain is located at the western margin of the McMurdo Volcanic Group (MMVG) which extends along the western Ross embayment. The great majority of the MMVG volcanic centers are within a distance of ~1000 km, which is the maximum distance for the source volcano of the Frontier Mountain tephra inferred from particle size. Two of the major volcanic provinces within MMVG are the Mount Melbourne (MMVP) and Mount Erebus (MEVP) provinces, which are located ~200 km due SE and ~600 km due S of Frontier Mountain, respectively. These provinces (Late Cenozoic–Holocene) were active during the building of the ice sheet that today covers the Antarctic continent (LeMasurier and Thomson, 1990). Figs. 6a, c and e show a good major element compositional match between the Frontier Mountain glass shards with MMVG. Fig. 7 also shows the same match for the trace element compositions of the FM2, FM3 B19 and B20 trachytic and tephritic glasses. In particular, the lack of the Ta–Nb hump in the primitive mantle normalized pattern of the more alkaline MEVP (see also Rocchi et al., 2002) suggests that the latter has a closer affinity to the MMVP. Figs. 6a, c and e also show that the Frontier Mountain glasses have a good major element geochemical affinity to rocks erupted from Mount Melbourne, Mount Rittman and The Pleiades. These volcanoes are the closest MMVG emission centers to Frontier Mountain (within a distance of ~200 km). Mount Melbourne and Mount Rittman have been active since the Pliocene (LeMasurier and Thomson, 1990; Bonaccorso et al., 1991), and The Pleiades have a well-documented history of pyroclastic activity, with 9 dated eruptions within the last 100 ka (Esser and Kyle, 2002) corresponding to the formation time interval estimated by us for the Frontier Mountain blue ice (see Section 5.1). As such, we conclude that the Frontier Mountain tephra were most likely generated within the

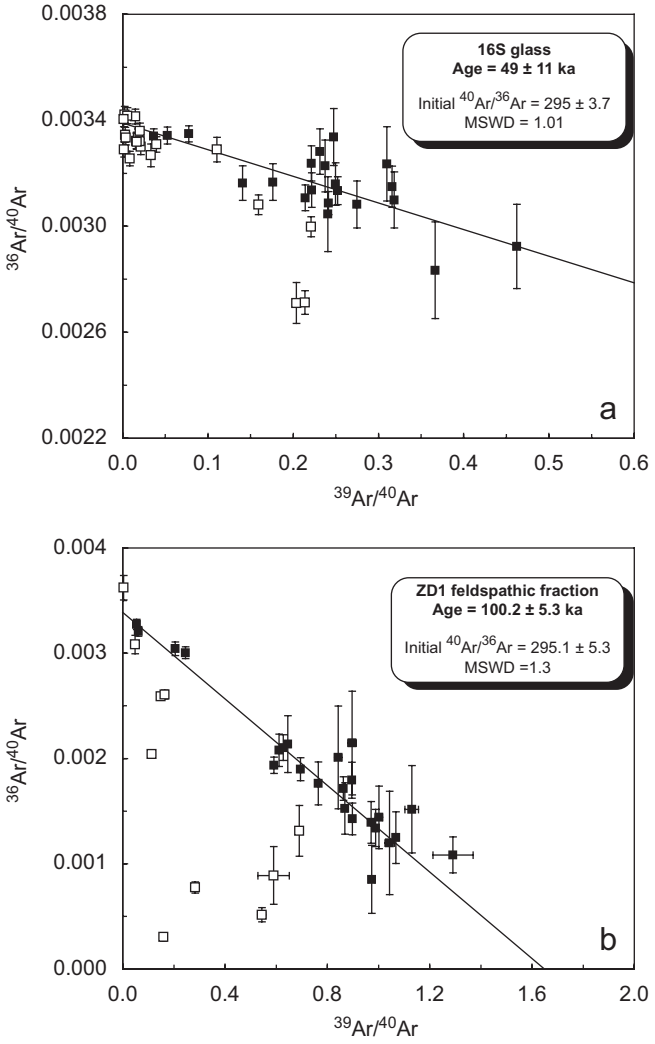

Fig. 9. Isotope correlation diagrams of 16 S dark glass (a) and ZD1 feldspathic fraction (b). The isochron ages are calculated on the same steps used in each analysis to calculate the plateau age (solid squares) (Table SM1 in Supplementary Material). Open squares represent the steps not used in the calculation. Error bars represent $\pm 1\sigma$ analytical error. Errors on isochron ages are at the $\pm 95\%$ conf. level.

MMVG, with the relatively close centers of the Mount Melbourne, The Pleiades and Mount Rittman as the most likely source volcanoes.

An interesting exercise is the comparison of the geochemical data for the 9 volcanic rocks erupted by The Pleiades during the last 100 ka (Kyle, 1982; Esser and Kyle, 2002) and the bulk compositions of the Frontier Mountain tephra layers. The Frontier Mountain 16S layer and the #25702 trachyte lava from The Pleiades show strikingly similar chemical compositions (see also Figs. 6a, c and e) and overlapping ^{40}Ar–^{39}Ar ages, namely 49 ± 11 and 48 ± 2 ka, respectively. As pyroclastic rocks are present throughout The Pleiades volcanic center (Esser and Kyle, 2002), we suggest that 16S is related to the volcanic activity of The Pleiades which generated the #25702 trachyte described in Kyle (1982). Additional data, e.g. direct glass-to-glass comparison, could confirm this correlation.

5.3. Implications for the regional stratigraphy of the Antarctic ice sheet

Englacial tephra layers are potential chronostratigraphic markers of the Antarctic ice sheet. Recently, Narcisi et al. (2006) reported the identification of one such layer in the EPICA-Dome C (sample 1265.1) and Dome Fuji ice cores, with a 86.7 ka model core age and, related it to a 92 ± 2.5 ka-old pyroclastic event of Mt. Berlin in Marie Byrd Land. This results stems out from a previous systematic study of 13 layers identified within the first 2150 m of the EPICA-Dome C (EDC) core, with model ages up to ~209 ka. Based on glass shards compositions Narcisi et al. (2005) attributed five layers to South Sandwich volcanoes, two layers to South Shetland volcanoes, two layers to Andean volcanoes, and four layers to the Marie Byrd Land (MBL) and Mount Melbourne volcanic provinces. Considering that the age of the Frontier Mountain blue ice (up to ~100 ka) partly overlaps the calculated time interval of the EDC core investigated by Narcisi et al. (2005), and that six tephra layers from EDC have calculated ages <100 ka (including the marker, ~92 ka, layer 1265.1), we investigated potential correlations, based on the geochemical composition of glass shards.

Compositional data shown in Table 3 (this work) and Table 2 of Narcisi et al. (2005) indicate that the trachytic Frontier Mountain sample B1 is similar to sample 1265.1 from the EDC core. In particular, they share similar alkali and silica contents, sodic (Na_2O–$2/K_2O$ ratio of 1.07 and 1.12 in B1 and 1265.1, respectively) and peralkaline (agpaitic index of 1.19 and 1.16 in B1 and 1265.1, respectively) characters (Figs. 6a, c and e). B1 is a layer from the northern ice flow (Fig. 3), occurring close to (and down-glacier of) the ZA–ZD1 layer with an ^{40}Ar–^{39}Ar age of 100 ± 5 ka. According to our stratigraphic reconstruction, the B1 level should be slightly older than ZA–ZD1; however, on considering the uncertainty associated with the age of ZA–ZD1 and the one derived for 1265.1 (Narcisi et al., 2005, 2006), their pairing is plausible. Given the significance of identifying regional- or continental-scale chronostratigraphic markers in the Antarctic ice sheets, it would be important to verify this pairing. The issue could be addressed by determining trace element compositions of the B1 glass shards and comparing them with those from 1265.1 (Narcisi et al., 2006). In addition, the B1 layer could be re-sampled in order to obtain enough material for ^{40}Ar–^{39}Ar age determination. As a by-product, this would also emphasize the importance of the blue-ice areas as natural deposits of suitable material for reconstructing the chronology of explosive eruption events.

The possible pairing of B1 with the 1265.1 layer raises the issue of the correct attribution to the source volcano, with important implications for volcanic ash transport mechanisms, the energy of volcanic explosions and wind regimes, and their regional-scale distribution. We ascribed B1 to the MMVG, whereas Narcisi et al. (2006) linked

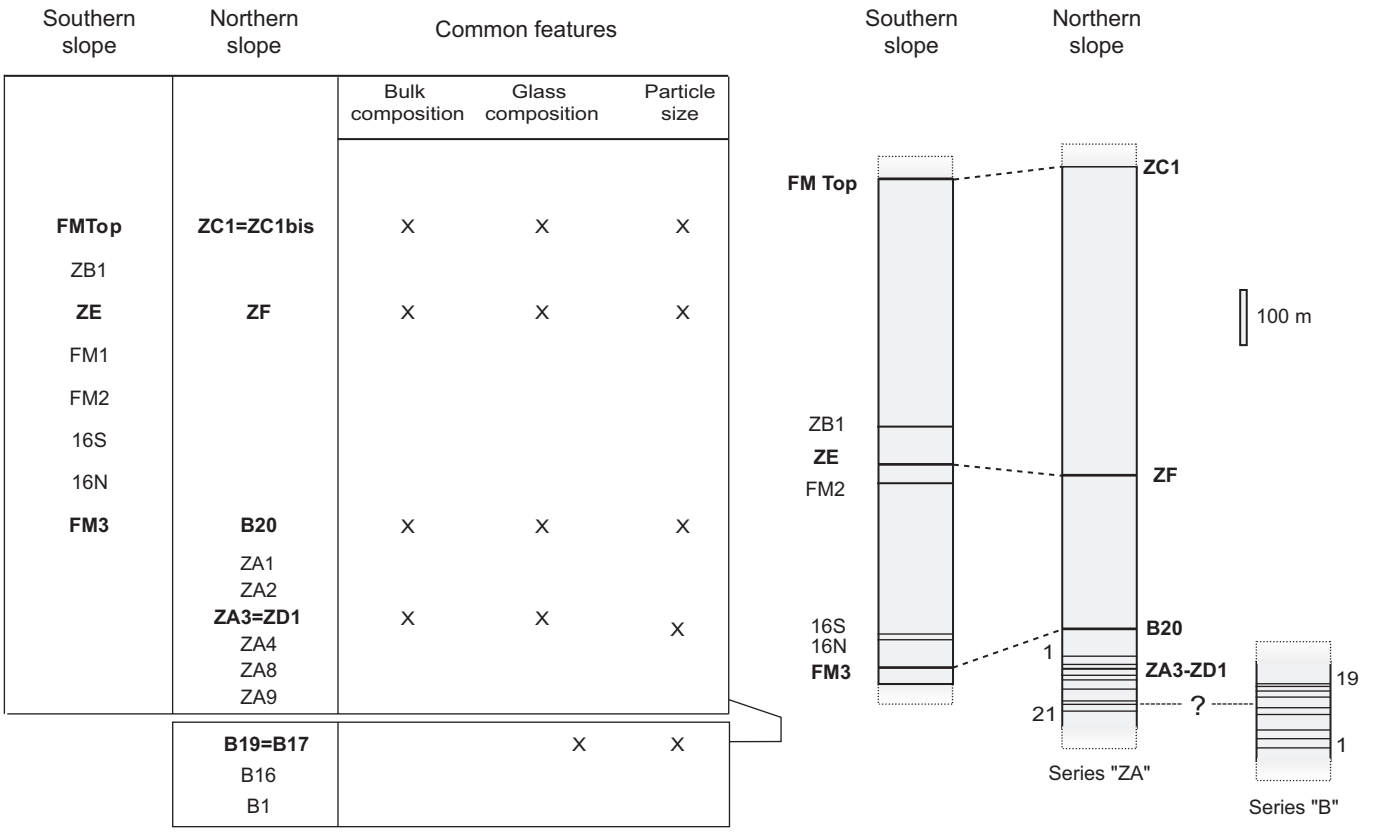

Fig. 10. (a) Morphometrical and compositional parameters of tephra layers from the Frontier Mountain blue-ice field, used to establish correlations between the northern and southern slope ice flows. (b) A tephra chronostratigraphic framework for the Frontier Mountain blue ice.

1265.1 to the explosive eruption of Mt. Berlin in MBL. Our attribution is based on the particle size and major element composition of glass shards whereas that by Narcisi et al. (2006) is based on their major and trace element composition, and on the 86.7 ka model core age. The large overlap in the major element composition of trachytes from the MMVG and MBL (Figs. 6a, c and e) and the 93 ± 4 ka-old trachytic eruption of The Pleiades (Esser and Kyle, 2002) would, at least in part, explain the dichotomy. Note also that Narcisi et al. (2006) use the REE, Sr and Nb concentrations as key elements for checking the consistency of their attribution to MBL; however, the database they refer to lists the compositions of merely 11 and four trachytic rocks and glass shards from MBL (Table 7.4 in LeMasurier and Rex, 1991, and Table 2 in Wilch et al., 1999) and Mount Melbourne (Table 2 in Wörner et al., 1989), respectively. In addition, trachytes with Sr and Nb concentration similar to those of the EDC 1265.1 glass, i.e. in the 0–20 and 100–300 ppm ranges, respectively, are, for instance, reported for the MMVP in LeMasurier and Thomson (1990): the Sr and Nb contents of an evolved trachyte from the Mount Melbourne summit are 14 and 176 ppm, respectively (see also sample MM16 in Table 2 of Wörner et al., 1989), i.e. undistinguishable from those of the 1265.1 glass (namely, $Sr = 8.88 \pm 7.45$ ppm and $Nb = 229 \pm 109$ ppm; see Table 2 in Narcisi et al., 2006). The existence of diagnostic elemental ratios for the different volcanic provinces should therefore be verified using comprehensive databases. We therefore suggest that the attribution of EDC 1265.1 glass to its parent emission center remains an open issue. In addition, accurate attributions to a specific eruption require direct glass-to-glass and/or rock-to-rock geochemical comparisons and, possibly, geochronological constraints.

A geochemical similarity is also observed between the FM1 glass from Frontier Mountain and the glass from the 1732.5 EDC layer described by Narcisi et al. (2005). They have similar trachytic composition with almost indistinguishable alkali and silica contents, and agpaitic index (Figs. 6a, c and e). However, the 1732.5 EDC layer has a model age of 129.5 ka. The FM1 layer, found on the southern ice flow ultimately leading to the Meteorite Moraine, should however be younger than $\sim 50 \pm 10$ ka; according to our stratigraphic reconstruction, the FM1 layer should be younger than the 16S layer which has a 49 ± 11 ka ^{40}Ar–^{39}Ar age.

Another implication of our result is that the many tephra layers embedded in the Frontier Mountain blue ice represent a ~ 100 ka continuous record of explosive volcanic activity in northern Victoria Land. Note also that in some cases (e.g. the ZA# or the B# sequences; Fig. 2a), tens of visible tephra are found within one hundred meters, offering the opportunity to study highly time-resolved sequences of explosive events. For instance it would be

possible to estimate the amount of material erupted during each event once distance from the emission center and amount of deposited ash at a given distance are known. Based upon a simplified and conservative model (emission center 200 km away from the deposition area, i.e. corresponding to the distance of The Pleiades and Mt. Melbourne, and a uniform ash distribution along a 20-km-wide stretch of ice in between), we estimate a minimal amount of 3.2×10^5 tons of dispersed ash during the event that produced the ZC1 layer (80 g per square meter), corresponding to 105 m^3 of erupted material.

Although tephra produced by catastrophic equatorial or low latitude eruptions may have a global correlation significance (Delmas et al., 1985), local events offer a much more concrete opportunity for correlation and dating. Deposits from local volcanic activity are much larger than those from remote events, as they are both more clearly visible and composed of larger particles. As such, the record of volcanic activity revealed by Frontier Mountain tephra could likely be found in other blue-ice areas as well as in deep-cores at a regional scale. The chronostratigraphic framework reported in this work represents the basis for a more detailed work in which all the Frontier Mountain layers could be included. Such a detailed chronostratigraphic reconstruction could be important in light of the ongoing ice core drilling project at Talos Dome (Frezzotti et al., 2004), where the same tephra layers are expected to be found. The identification of paired tephra layers may in fact help define regional-scale chronostratigraphic correlations from snow accumulation zones to ablation areas in the Talos Dome–Rennick Glacier area, thus offering an additional tool for studying ice dynamics. In addition, the Frontier Mountain blue ice may become a potential site for sampling selected ice successions for high-resolution past atmospheric chemistry and fallout, such as those around the Last Interglacial–glacial–interglacial transition which are of great scientific interest for paleoclimatic studies of the recent geological past.

5.4. Implications for the meteorite concentration mechanism at Frontier Mountain

About 500 meteorite specimens have been found to date on the southern and northern slopes of the Frontier Mountain blue-ice field (www.mna.it). Welten et al. (2001, 2006) have shown that all of the 11 and 18 specimens so far dated from the southern and northern slopes have terrestrial ages of up to 40 ± 10 and 140 ± 30 ka, respectively. These ages match the ages of ~50 and ~100 ka derived in this work for the ice successions under ablation on the northern and southern slopes, respectively. One possible interpretation of this result is that a mechanism of exhumation of meteorites by ablation after englacial transport from snow accumulation areas is actually at work at Frontier Mountain, supporting previous works (e.g., Cassidy et al., 1992; Folco et al., 2002).

6. Summary and conclusions

1. Structural, mineralogical, geochemical and geochronological data on englacial tephra layers allowed us to reconstruct a glacial chronostratigraphic framework of the Frontier Mountain blue-ice field. To our knowledge, this is the first tephra chronostratigraphic reconstruction of an Antarctic blue-ice area.
2. The geometry of the tens of tephra layers mapped in the field allowed us to define the overall structure of the two ice flows nourishing the Frontier Mountain blue-ice field. In particular, both the ice flow from the south and the one from the north can be described as up-glacier homoclines (with severe deformation only at their fronts).
3. The mineralogical, morphometrical and geochemical analysis of 22 representative layers demonstrated that each layer has characteristic features which enable us to define coherent ice successions and establish stratigraphic correlations amongst the two ice flows. The calculated stratigraphic thickness of the ice succession cropping out at the Frontier Mountain blue ice is ~1150 m. This succession is entirely exposed at the surface of the northern flow; only the first ~1000 m of the succession crop out at the surface of the southern flow.
4. Two tephra layers were dated using the ^{40}Ar–^{39}Ar geochronological method. The age of one layer close to the stratigraphic bottom of the ice succession is 100 ± 5 ka and constrains the maximum age of the bulk of Frontier Mountain blue ice. The age of the second layer at a depth of ~950 m in the stratigraphic succession indicates that >90% of the ice currently under ablation at Frontier Mountain is younger than 49 ± 11 ka.
5. Particle size and compositional data relate the 22 sampled layers to alkaline source volcanoes within the West Antarctic Rift System. In particular, the relatively large particle size (up to several tens of microns) indicates a proximal source. Geochemical and geochronological data match literature data for the Mount Melbourne, Mount Rittman and The Pleiades lavas, suggesting that these three emission centers (amongst the closest centers to Frontier Mountain, within a ~250 km radius) are the best candidate source volcanoes. Note the possible correlation between the 49 ± 11 ka-old 16S tephra layer and a 48 ± 2 ka trachytic eruption from The Pleiades (sample #25702; see Kyle, 1982; Esser and Kyle, 2002). The chronostratigraphic framework of the Frontier Mountain blue-ice field here reported lays the foundations for a detailed reconstruction of ~100 ka of explosive volcanism in northern Victoria Land.
6. In light of the ongoing ice core drilling project at Talos Dome (Frezzotti et al., 2004), the Frontier Mountain ice succession may become important for establishing regional-scale correlations from snow accumulation to

ablation zones in the Rennick Glacier area, for calibrating time–depth profiles of the ice sheet through sampling and dating of key tephra layers, and for high-resolution past atmospheric chemistry and fallout through sampling of selected ice successions. In particular, the successions around the Last Interglacial–glacial–interglacial transition are currently of great scientific interests for paleoclimatic studies.

7. Comparison of the geochemical and geochronological data of the Frontier Mountain tephra with those found in the EDC core (Narcisi et al. 2005, 2006) raises the possibility that The Pleiades volcanic center is the source for EDC sample 1265.1, formerly considered a chronostratigraphic marker correlated with Mt. Takahe in MBL (Narcisi et al., 2006). This issue highlights the need for comprehensive geochemical and geochronological databases to be used in establishing correlations between tephra layers and source volcanoes.
8. The fact that the age of the Frontier Mountain blue ice overlaps with terrestrial ages of meteorites found thereon (up to 140 ± 30 ka; Welten et al., 2001, 2006) is consistent with a mechanism of exhumation of meteorites in the blue-ice field by ablation after englacial transport from snow accumulation areas (e.g., Cassidy et al., 1992; Folco et al., 2002).

Acknowledgments

This work was supported by the Italian *Programma Nazionale delle Ricerche in Antartide* (PNRA) and *Consiglio Nazionale delle Ricerche* (CNR). G. De Grandis (IGG-CNR-Pisa) is thanked for her help in mineral separation. The manuscript benefited from the careful reviews of W.E. LeMasuerier and P.R. Kyle. The Associate Editor, E. Brook, is thanked for editorial assistance.

Appendix A. Supplementary data

The online version of this article contains additional supplementary data. Please visit doi:10.1016/j.quascirev.2007.11.017

References

Armienti, P., Tripodo, A., 1991. Petrography and chemistry of lavas and comagmatic xenoliths of M. Rittman, a volcano discovered during the IV Italian expedition in Northern Victoria Land (Antarctica). Memorie della Società Geologica Italiana 46, 427–451.

Basile, I., 1997. Origine des aérosol volcaniques et continentaux de la carotte de glace de Vostok (Antartique). Thése de doctorat, Université Joseph Fourier-Grenoble I, France.

Basile, I., Petit, J.R., Touron, S., Grousset, F.E., Barkov, N., 2001. Volcanic layers in Antarctic (Vostok) ice cores: source identification and atmospheric implications. Journal of Geophysical Research 106 (D23), 31.915–31.931.

Behrendt, J.C., LeMasurier, W.E., Cooper, A.K., Tessensohn, F., Trehu, A., Damaske, D., 1991. Geophysical studies of the West Antarctic rift system. Tectonics 10, 1257–1273.

Bence, A.E., Albee, A.L., 1968. Empirical correction factors for the electron microanalysis of silicates and oxides. Journal of Geology 76, 382–403.

Bintanja, R., 1999. On the glaciological, meteorological, and climatological significance of Antarctic blue ice areas. Reviews of Geophysics 37, 337–359.

Bonaccorso, A., Mione, M., Pertusati, P.C., Privitera, E., Ricci, C.A., 1991. Fumarolic activity at Mt. Rittman volcano (Northern Victoria Land, Antarctica). Memorie della Società Geologica Italiana 46, 453–456.

Cassidy, W., Harvey, R., Shutt, J., Delisle, G., Yanai, K., 1992. The meteorite collection sites of Antarctica. Meteoritics 27, 490–525.

Delisle, G., Shultz, L., Spettel, B., Weber, H.W., Wlotzka, F., Hofle, H.C., Thierback, R., Vogt, S., Herpers, U., Bonani, G., Suter, M., Wolfli, W., 1989. Meteorite finds near the Frontier Mountain Range in North Victoria Land. In: Damaske, D., Durbaum, H.J. (Eds.), GANOVEX VI Herausgegeben von der Bundesanstalt für Geowissenshaften und Rohstoffe. Geologisches Jahrbuch E38, 369–393.

Delmas, R.J., Legrand, M., Aristarain, A.J., Zanolini, F., 1985. Volcanic deposits in Antarctic snow and ice. Journal of Geophysical Research 90 (D7), 12901–12920.

Deponti, A., Maggi, V., 2002. Talos dome age vs. depth modelling, Terra Antarctica Report, 8, pp. 113–117.

Dunbar, N.W., Kyle, P.R., McIntosh, W.C., Esser, R.P., 1995. Geochemical composition and stratigraphy of tephra layers in Antarctic blue ice: insights into glacial tephrochronology. In: VII International Symposium on Earth Sciences, Siena, September 1995, p. 115.

Dunbar, N.W., Zielinsky, G.A., Voisin, D.T., 2003. Tephra layers in the Siple and Taylor Dome ice cores, Antarctica: sources and correlations. Journal of Geophysical Research 108 (B8), 2374 ECV 6, 1–11.

Esser, R.P., Kyle, P.R., 2002. $^{40}Ar/^{39}Ar$ chronology of the McMurdo Volcanic group at the Pleiades, northern Victoria land, Antarctica. Royal Society of the New Zealand Bulletin 35, 415–418.

Folco, L., Capra, A., Chiappini, M., Frezzotti, M., Mellini, M., Tabacco, I.E., 2002. The Frontier Mountain meteorite trap (Antarctica). Meteoritics and Planetary Science 37, 209–228.

Folco, L., Welten, K.C., Jull, A.J.T., Nishiizumi, K., Zeoli, A., 2006. Meteorites constrain the age of the Frontier Mountain blue ice field (northern Victoria Land). Earth and Planetary Science Letters 248, 209–216.

Frezzotti, M., Bitelli, G., De Michelis, P., Deponti, A., Forieri, A., Gandolfi, S., Maggi, V., Mancini, F., Rémy, F., Tabacco, I.E., Urbini, S., Vittuari, L., Zirizzotti, A., 2004. Geophysical survey at Talos Dome East Antarctica: the search for a deep new drilling site. Annals of Glaciology 39, 423–432.

Fujii, Y., Kohno, M., Motoyama, H., Matoba, S., Watanabe, O., Fujita, S., Azuma, N., Kikuchi, T., Fukuoka, T., 1999. Tephra layers in the Dome Fuji (Antarctica) deep ice core. Annals of Glaciology 29, 126–130.

Gow, A.J., Williamson, T., 1971. Volcanic ash in the Antarctic ice sheet and its possible climatic implications. Earth and Planetary Science Letters 13, 210–218.

Gunn, B.M., Warren, G., 1962. Geology of Victoria Land between the Mawson and Mulock Glaciers, Antarctica. Bulletin of the Geological Survey of New Zealand 71, 157.

Hammer, C.U., Clausen, H.B., Langway Jr., C.C., 1997. 50000 years of recorded global volcanism. Climatic Change 35, 1–15.

Harvey, R.P., 2003. The origin and significance of Antarctic meteorites. Chemie der Erde 63, 93–147.

Harvey, R.P., Dunbar, N.W., McIntosh, W.C., Esser, R.P., Nishiizumi, K., Taylor, S., Caffee, M.W., 1998. Meteoritic event recorded in Antarctic ice. Geology 26 (7), 607–610.

Heizler, M.T., Peryy, F.V., Crowe, B.M., Peters, L., Appelt, R., 1999. The age of Lathrop Wells volcanic center: an $^{40}Ar/^{39}Ar$ dating investigation. Journal of Geophysical Research 104, 767–804.

Higashi, A., Fujii, Y., 1994. Studies on microparticles contained in medium-depth ice cores retrieved from east Dronning Maud Land, Antarctica. Annals of Glaciology 20, 73–79.

Juvigne, E., Porter, S.C., 1985. Mineralogical variations within two widespread Holocene tephra layers from Cascade Range Volcanoes, USA. Geographie Physique et Quatèrnaire 39, 7–12.

Katsushima, T., Nishio, F., Ohmae Hishikawa, M., Takahashi, S., 1984. Composition of dirt layers in the bare ice areas near the Yamato Mountains in Queen Maud Land and the Allan Hills in Victoria Land, Antarctica. Memoirs of National Institute of Polar Research, Special Issue 34, 174–187.

Keys, J.R., Anderton, P.W., Kyle, P.R., 1977. Tephra and debris layers in the Skelton Nevè and Kempe Glacier, South Victoria Land, Antarctica. New Zealand Journal of Geology and Geophysics 20, 71–1002.

Koeberl, C., 1988. Volcanic ash layers in blue ice fields (Beardmore Glacier area, Antarctica): iridium enrichments. Lunar and Planetary Contribution 673, 93–94.

Koeberl, C., 1990. Dust bands in blue ice fields in Antarctica and their relationship to meteorite and ice. In: Cassidy, W.A., Whillans, I.M. (Eds.), Workshop on Antarctic Meteorite Stranding Surfaces. Lunar and Planetary Institute Technical Report, 90, 03, pp. 70–73.

Koeberl, C., Yanai, K., Cassidy, W.A., Schutt, J.W., 1988. Investigation of dust bands from blue ice fields in the Lewis Cliff (Beardmore) area, Antarctica: a progress report. In: Proceedings of NIPR Symposium Antarctic Meteorites, vol. 1, pp. 291–309.

Kurbatov, A.V., Dunbar, N.W., Zielinski, G.A., Mayewski, P.A., Curran, M.A., Morgan, V., van Ommen, T.D., 2003. Evaluation of Tephra Found in the Law Dome Ice Core, East Antarctica. Eos Transactions AGU 84(46), Fall Meeting Supplement, Abstract A31C-56.

Kyle, P.R., 1982. Volcanic geology of The Pleiades, Northern Victoria Land, Antarctica. In: Craddock, C. (Ed.), Antarctic Geoscience. University of Wisconsin Press, Madison, pp. 747–754.

Kyle, P.R., Rankin, P.C., 1976. Rare earth elements geochemistry of Late Cenozoic alkaline lavas of the McMurdo Volcanic Group, Antarctica. Geochimica et Cosmochimica Acta 40, 1497–1507.

Kyle, P.R., Jezek, P.A., Mosley-Thompson, E., Thompson, L.G., 1981. Tephra layers in the Byrd station ice core and the Dome C ice core, Antarctica and their climatic importance. Journal of Volcanology and Geothermal Research 11, 29–39.

Kyle, P.R., Palais, J., Delmas, R., 1982. The volcanic record of Antarctic ice cores: preliminary results and potential for future investigations. Annals of Glaciology 3, 172–177.

Kyle, P.R., Palais, J., Thomas, E., 1984. Vostok tephra—an important englacial stratigraphic marker? Antarctic Journal of United States 19, 64–65.

Le Bas, M.J., Le Maitre, R.W., Streckeisen, A., Zanettin, B., 1986. A chemical classification of volcanic rocks based on the total alkali-silica diagram. Journal of Petrology 27, 745–750.

LeMasurier, W.E., Rex, D.C., 1989. Evolution of linear volcanic ranges in Marie Byrd Land, West Antarctica. Journal of Geophysical Research 94, 7223–7236.

LeMasurier, W.E., Rex, D.C., 1991. Marie Byrd Land volcanic province and its relation to the Cenozoic West Antarctic rift system. In: Tingey, R.J. (Ed.), The Geology of Antarctica. Oxford University Press, Oxford, UK, pp. 249–284.

LeMasurier, W.E., Thomson, J.W., 1990. Volcanoes of the Antarctic Plate and Southern Oceans. Antarctic Research Series 48. American Geophysical Union, Washington, DC, p. 487.

Lisitzin, A.P., 1996. Volcanogenic sedimentation. In: Oceanic Sedimentation Lithology and Geochemistry (English translation edited by J.P. Kennett). American Geophysical Union, Washington, DC, pp. 322–335.

MacDonald, G.A., Katsura, T., 1964. Chemical composition of Hawaiian lavas. Journal of Petrology 5, 82–133.

Marvin, U.B., 1986. Components of dust bands in ice from cul de sac, Allan Hills region, Antarctica. Lunar and Planetary Institute Contribution 600 (R-9), 442–443.

McDonough, W.F., Sun, S., 1995. The composition of the Earth. Chemical Geology 120, 223–253.

Narcisi, B., Proposito, M., Frezzotti, M., 2001. Ice record of a 13th century explosive volcanic eruption in Northern Victoria Land, East Antarctica. Antarctic Science 13 (2), 174–181.

Narcisi, B., Petit, J.R., Del Monte, B., Basile-Doelsch, I., Maggi, V., 2005. Characteristics and sources of tephra layers in the EPICA-Dome C ice record (East Antarctica): implications for past atmospheric circulation and ice core stratigraphic correlations. Earth and Planetary Science Letters 239, 253–265.

Narcisi, B., Petit, J.R., Tiepolo, M., 2006. A volcanic marker (92 ka) for dating deep east Antarctic ice cores. Quaternary Science Reviews 25, 2682–2687.

Naruse, R., Hashimoto, M., 1982. Internal flow lines in the ice sheet upstream of the Yamato Mountains, East Antarctica (extended abstract). In: Kusunoki, K. (Ed.), Proceedings of the Fourth Symposium on Polar Meteorology and Glaciology. Memoirs of National Institute of Polar Research, Special Issue 24, 201–203.

Nishio, F., Katsushima, T., Ohmae, H., 1985. Volcanic ash layers in bare ice areas near the Yamato Mountains, Dronning Maud Land and the Allan Hills, Victoria Land, Antarctica. Annals of Glaciology 7, 34–41.

Palais, J.M., 1985. Particle morphology, composition and associated ice chemistry of tephra layers in the Byrd ice core: evidence for hydrovolcanic eruptions. Annals of Glaciology 7, 42–48.

Palais, J.M., Kyle, P.R., McIntosh, W.C., Seward, D., 1988. Magmatic and phreatomagmatic volcanic activity at Mt. Takahe, West Antarctica, based on tephra layers in the Byrd Ice Core and field observations at Mt. Takahe. Journal of Volcanology and Geothermal Research 35, 295–317.

Palais, J.M., Petit, J.R., Lorius, C., Korotkevich, Y.S., 1989. Tephra layers in the Vostok ice core: 160,000 years of southern hemisphere volcanism. Antarctic Journal of United States XX, 98–100.

Perchiazzi, N., Folco, L., Mellini, M., 1999. Volcanic ash bands in the Frontier Mountain and Lichen Hills blue-ice fields, northern Victoria Land. Antarctic Science 11 (3), 353–361.

Rocchi, S., Armenti, P., D'Orazio, M., Tonarini, S., Wijbrans, J.R., Di Vincenzo, G., 2002. Cenozoic magmatism in the western Ross Embayment: role of mantle plume versus plate dynamics in the development of the West Antarctic Rift System. Journal of Geophysical Research 107 (B9), 2195.

Smellie, J.L., 1999. The upper Cenozoic tephra record in the south polar region: a review. Global and Planetary Change 21, 51–70.

Welten, K.C., Nishiizumi, K., Masarik, J., Caffee, M.W., Jull, A.J.T., Klandrud, S.E., Wieler, R., 2001. Cosmic-ray exposure history of two Frontier Mountain H-chondrite showers from spallation and neutron-capture product. Meteoritics and Planetary Science 36, 301–317.

Welten, K.C., Nishiizumi, K., Caffee, M.W., Hillegonds, D.J., Johnson, J.A., Jull, A.J.T., Wieler, R., Folco, L., 2006. Terrestrial ages and pairing of Antarctic chondrites from Frontier Mountain, northern Victoria Land. Meteoritics and Planetary Science 41, 1081–1094.

Whillans, I.M., Cassidy, W.A., 1983. Catch a falling star: meteorites on old ice. Science 222, 55–57.

Wilch, T.I., McIntosh, W.C., Dunbar, N.W., 1999. Late Quaternary volcanic activity in Marie Byrd land: potential $^{40}Ar/^{39}Ar$-dated time horizons in West Antarctic ice and marine cores. Geological Society of America Bulletin 111 (10), 1563–1580.

Wörner, G., Viereck, L., Hertogen, J., Niephaus, H., 1989. The Mt Melbourne Volcanic Field (Victoria Land, Antarctica) II, Geochemistry and magma genesis. In: Damaske, D., Durbaum, H.J. (Eds.), GANOVEX VI Herausgegeben von der Bundesanstalt für Geowissenshaften und Rohstoffe. Geologisches Jahrbuch E38, 395–433.

Zeoli, A., 2002. Concentrazioni di meteoriti e dinamica glaciale in Antartide: la trappola di Frontier Mountain. Ph.D. Thesis, Università degli Studi di Siena, Italy.